

# Accepted Manuscript

Novel Tacrine-Hydroxyphenylbenzimidazole hybrids as potential multitarget drug candidates for Alzheimer's disease

Asha Hiremathad, Rangappa S. Keri, A. Raquel Esteves, Sandra M. Cardoso, Sílvia Chaves, M. Amélia Santos



PII: S0223-5234(18)30151-X

DOI: [10.1016/j.ejmech.2018.02.023](https://doi.org/10.1016/j.ejmech.2018.02.023)

Reference: EJMECH 10200

To appear in: *European Journal of Medicinal Chemistry*

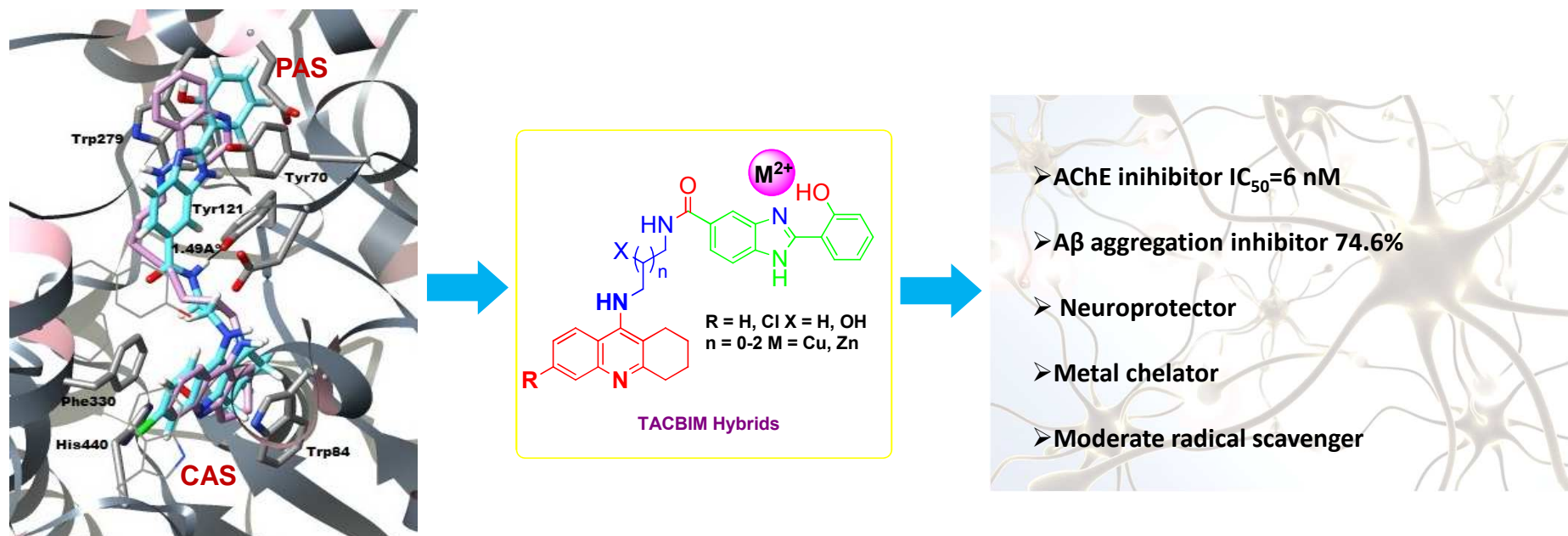
Received Date: 4 October 2017

Revised Date: 7 February 2018

Accepted Date: 8 February 2018

Please cite this article as: A. Hiremathad, R.S. Keri, A.R. Esteves, S.M. Cardoso, Sílvia Chaves, M. Amélia Santos, Novel Tacrine-Hydroxyphenylbenzimidazole hybrids as potential multitarget drug candidates for Alzheimer's disease, *European Journal of Medicinal Chemistry* (2018), doi: 10.1016/j.ejmech.2018.02.023.

This is a PDF file of an unedited manuscript that has been accepted for publication. As a service to our customers we are providing this early version of the manuscript. The manuscript will undergo copyediting, typesetting, and review of the resulting proof before it is published in its final form. Please note that during the production process errors may be discovered which could affect the content, and all legal disclaimers that apply to the journal pertain.



Multitargeting **TAC-BIM** hybrids as anti-Alzheimer's disease agents

# Novel Tacrine-Hydroxyphenylbenzimidazole Hybrids as Potential Multitarget Drug Candidates for Alzheimer's Disease

Asha Hiremathad,<sup>a,b</sup> Rangappa S. Keri,<sup>b\*</sup> A. Raquel Esteves,<sup>c,d</sup> Sandra M. Cardoso,<sup>c,d</sup> Sílvia Chaves,<sup>a</sup> M. Amélia Santos<sup>a\*</sup>

<sup>a</sup> Centro de Química Estrutural, Instituto Superior Técnico, Universidade de Lisboa, Av. Rovisco Pais 1, 1049-001 Lisboa, Portugal; <sup>b</sup> Centre for Nano and Material Sciences, Jain University, Jain Global Campus, Kanakapura, Ramanagara, Bangalore 562112, India; <sup>c</sup> CNC—Center for Neuroscience and Cell Biology, University of Coimbra, Coimbra, Portugal; <sup>d</sup> Institute of Cell and Molecular Biology, Faculty of Medicine, University of Coimbra, Coimbra, Portugal.

## Abstract

Alzheimer's disease (AD) is a severe age-dependent neurodegenerative disorder affecting millions of people, with no cure so far. The current treatments only achieve some temporary amelioration of the cognition symptoms. The main characteristics of the patient brains include the accumulation of amyloid plaques and neurofibrillary tangles (outside and inside the neurons) but also cholinergic deficit, increased oxidative stress and dyshomeostasis of transition metal ions. Considering the multi-factorial nature of AD, we report herein the development of a novel series of potential multi-target directed drugs which, besides the capacity to recover the cholinergic neurons, can also target other AD hallmarks. The novel series of tacrine-hydroxyphenylbenzimidazole (TAC-BIM) hybrid molecules has been designed, synthesized and studied for their multiple biological activities. These agents showed improved AChE inhibitory activity ( $IC_{50}$  in nanomolar range), as compared with the single drug tacrine (TAC), and also a high inhibition of self-induced- and Cu-induced- $A\beta$

aggregation (up to 75%). They also present moderate radical scavenging activity and metal chelating ability. In addition, neuroprotective studies revealed that all these tested compounds are able to inhibit the neurotoxicity induced by A $\beta$  and Fe/AscH(-) in neuronal cells. Hence, for this set of hybrids, structure-activity relationships are discussed and finally it is highlighted their real promising interest as potential anti-AD drugs.

**Keywords:** Alzheimer's disease; multitarget compounds; Tacrine hybrids; dual binding site AChE inhibitors; anti amyloid aggregation

## 1. Introduction

Alzheimer's disease (AD) is by far the most common cause of dementia in the elder population. It is characterized by short and long term memory loss, resulting in severe cognition and functional impairment, behavioral and mental disorientation. The growth of this disease is of major concern to the worldwide society. According to a recent report by WHO, there are approximately 47.5 million individuals affected from this dementia and its prevalence is expected to continue growing up to be 135.5 million by 2050 [1,2].

AD patients have some areas of the brain, namely cerebral cortex and hippocampus, which are particularly vulnerable to neuron degeneration and loss [3,4]. The main features of AD patient brains are the deposits of senile plaques of A $\beta$  peptides outside the neurons [5] and agglomerates (tangles) of hyperphosphorylated Tau protein within the neurons [6]; the deficit of cholinergic neurons resulting also from hydrolysis of acetylcholine (ACh) by acetylcholinesterase (AChE) [7,8]; and other prominent features such as increased oxidative stress [9] and imbalances in the homeostasis of metal ions [10-12].

The currently approved anti-AD drugs have been focused on recovering memory, mainly by improving the cholinergic defect by AChE inhibition [13]. However, they only achieve some temporary amelioration of the symptoms but do not interfere in the disease progress and so there is no cure so far [14]. Therefore, effective therapeutics are urgently needed. One of the main drawbacks in discovery of efficient drugs to treat AD has been the complexity of the disease and the lack of understanding about the pathogenesis of the disease. Accordingly, it has been realized that the key task of the effective drugs is to control the AD pathogenesis [12,14]. Thus, due to the complex multifactorial nature of AD, the paradigm of multitarget-directed drugs has recently emerged in drug development strategies [15-19]. In particular, aimed to treat the disease symptoms and also to control its progression, an extensive search has been made on repositioning AD drugs (inhibitors of AChE), based on their derivatization (hybridization) to endow them with capacity for hitting several disease targets [18]. In this context, herein we report the development of a series of tacrine (TAC) - hydroxyphenylbenzimidazole (BIM) conjugates or hybrids as potential pleiotropic anti-AD agents. TAC, as the first approved AChE inhibitor drug [20], was selected as the main scaffold. Regarding the BIM moiety, its selection envisages to endow the hybrids with capacity for hitting several AD targets. Although, a number of small molecules have been developed to study the metal-associated A $\beta$  species in AD [11,12,21], the aromatic and *N,O*-

donor chelating nature of this new moiety, will award the conjugate molecule with multiple roles, such as inhibition of the self- and Cu-induced A $\beta$  aggregation, as well as radical scavenging and metal chelating capacity. Furthermore, depending on the selected linker between the two main scaffolds, the BIM moiety can potentially provide extra favorable interaction within the active site of AChE, as compared with the single TAC drug.

Thus, aided by molecular simulations, a series of novel TAC-BIM conjugates have been designed and developed, as described in Fig. 1. Subsequently they have been studied for their important biological properties, namely inhibition of AChE and A $\beta$  aggregation, radical scavenging activity and also neuroprotective effects on neuronal cells subjected to AD stressors. The results are discussed based on structure-activity relationships, envisaging the outlining of the most prominent compounds as potential multitarget anti-AD drug candidates.

## 2. Results and Discussion

### 2.1. Molecular design and modeling

The design of the novel hybrids, to be subsequently prepared and studied, involved a preliminary selection of two main molecular scaffolds or pharmacophore elements, to assure the hitting of at least two main pathophysiological targets of AD pathology. Thus, tacrine (TAC) and hydroxyphenylbenzimidazole (BIM) were chosen as the main moieties. TAC was selected to guarantee the inhibition of AChE, while the BIM unit was included mainly due to its expected capacity to interact with A $\beta$  peptide and inhibit its self- and copper-induced aggregation due to its metal chelating capacity. Furthermore, if these two main molecular units are connected with adequate linkers, the corresponding hybrids can potentially act as bimodal AChE inhibitors with improved efficacy. Therefore, the selection of adequate linkers was aided by docking molecular simulations. The docking results indicated that the linker with two to three methylene groups could provide the hybrid with enough chain length to enable the dual interaction mode of both main scaffolds (TAC, BIM) within the enzyme gorge. Further studies confirm that these dihybrids could bind both catalytic anionic site (CAS) and peripheral anionic site (PAS) as shown in Fig. 2 as well as Fig. S1 and Fig. S2). The TAC moiety (superimposed with that of the original ligand) is well inserted in the CAS with a  $\pi$ - $\pi$  stacking interaction with Trp84 and Phe330, while the secondary amine proton of the linker

could form an hydrogen bond with Tyr121 and block the accessibility of substrate and water to the active site (formed by the catalytic triad Ser200, His440 and Glu327) [22]. Although His440 has been reported to interact with the pyridinic nitrogen of tacrine, this is not clear from our docking images, which can be due to the herein selected image view or eventually to an artifact of the simulation because protonation states, were not considered. The chloro substitution in TAC is supposed to lead to improvement of the enzyme inhibition, due to the good fitting of the chlorine atom in a hydrophobic pocket of *TcAChE* formed by Trp432, Met436 and Ile439 [23], otherwise identically reported for the human AChE (*hAChE*) [24]. In fact, from Fig 2A only the first residue (Trp432) can be seen in a close distance from the chlorine atom.

Similarly to the original ligand (Fig. S3), the BIM moiety could interact with PAS establishing a  $\pi$ - $\pi$  binding with Trp279 and Tyr70 (Fig. 2 and Fig. S3). The structure found for these hybrid-enzyme complex is pretty similar to the reported crystal structure of *TcAChE* complexed with tacrine-quinoline inhibitor (*N*-4'-quinoly-1-yl-*N'*-9''-(1'',2'',3'',4''-tetrahydroacridinyl)-1,8-diaminooctane; PDB entry 1ODC) [25] as shown in Fig. 2A for **11d**. These simulations also revealed that, among all the hybrids, compound **11d** showed the highest inhibitory capacity which may be rationalized by its dual binding with CAS and PAS, particularly, through the  $\pi$ - $\pi$  stacking with three aromatic residues (Trp279, Tyr70 and Tyr121). Furthermore, these simulations also indicated that the best bimodal interaction was accomplished for linkers with  $n = 0$  and 1 (with 2 and 3 methylene groups), although the corresponding H-bond interactions with Tyr121 (1.49 and 1.59 Å respectively) suggest that the hybrids with 2-methylene linker might establish a stronger interaction with the enzyme. The docking of the compound with 4-methylene linker (**9f**) indicates a longer H-bond distance (2.29 Å) as well as the positioning of the BIM moiety slightly away from PAS, thus signifying lower  $\pi$ - $\pi$  stacking interaction, hence lower enzymatic inhibition (Fig. 2B). The effect of the

hydroxyl group substituent in the linker was evaluated, based on comparison of simulation results of homologous compounds, which just differ in the presence or absence of that group (**12a** and **11b**). Analysis of Fig. 2C shows that the hydroxyl group of **12a** can establish an H-bond interaction (1.61 Å) with Asp72, which may contribute to the enzyme inhibition improvement [26]. Interestingly, docking results of compounds **11b** and **11e** (n = 1) also showed good  $\pi$ - $\pi$  stacking between BIM and aromatic amino acid residues of PAS, while the phenolic hydroxyl is forming H-bond with Glu278 (2.74 Å for **11b**), hence supporting a good enzyme inhibitory capacity (see Fig. 2D).

Overall, molecular simulations have shown good information about the interaction between the designed drug and the targeted enzyme. This shows that the designed molecules should present a very good AChE inhibition.

## 2.2. Chemistry

The novel tacrine-hydroxyphenylbenzimidazole (TAC-BIM) hybrids were prepared by the synthetic strategy outlined in Scheme 1. The tacrine starting molecules, 9-chloro-1,2,3,4-tetrahydroacridine **3(a-b)**, were prepared from commercially available anthranilic acids as previously reported [27,28]. Afterwards, compounds **3(a-b)** were attached at the 9-position to alkane-diamines and 1,3-diaminopropan-2-ol linkers in the presence of phenol and a catalytic amount of potassium iodide. The completion of the reaction was monitored by thin layer chromatography (TLC) and the product was purified by column chromatography to yield intermediate TAC amines **6(a-f)** and **7(a-b)**. The hydroxyphenylbenzimidazole acid was prepared by cyclization of 3,4-diamino benzoic acid and salicylaldehyde in the presence of DMA and sodium metabisulfite [29]. Finally the intermediates TAC-amines, **6(a-f)**, **7(a-b)** and the hydroxyphenylbenzimidazole acid (**10**) were coupled to each other *via* amide bond formation. This reaction was carried out in dry DMF with NHS and DCC as activators, under N<sub>2</sub> atmosphere for two days, affording the novel TAC-BIM hybrids.

## 2.3. Biological activity

### 2.3.1. AChE inhibition

Inhibition of *TcAChE* by the newly synthesized hybrids **11(a-f)** and **12(a-b)** was evaluated by adaptation of a method previously described [30]. The  $IC_{50}$  values for AChE inhibition are depicted in **Table 1**. These compounds, especially those with smaller chain linkers ( $n = 0-1$ ), appeared as excellent inhibitors, exhibiting inhibitory activity in nanomolar range, thus much higher than the standard drug (tacrine). Among all hybrids, compound (**11d**), with chloro-substitution and a two methylene linker, showed the highest inhibitory activity ( $IC_{50} = 6.3$  nM), which may be due to the adequate linker size and/or also to the TAC-Cl substituent. In fact, as expected, all the chloro-TAC hybrids, except **12b**, showed better inhibitory activity than the corresponding unsubstituted hybrids, which in some cases can attain differences of almost one order of magnitude (e.g. **11d** and **11a**). Concerning the effect of the size of the linker between the two main moieties, as anticipated by the molecular design simulations, it is a very important parameter in the enzyme inhibition, since it may determine the ability of the compounds for bimodal interaction within the AChE active site and thus increase the enzyme inhibition as compared with the mono-modal interaction of the drug (TAC). Comparison of the inhibitory activities ( $IC_{50} = 6.3, 23.7, 142$  nM) of homologous compounds (**11d**, **11e**, **11f**) with different size chain ( $n = 0-2$ ), shows that, although only small differences can still be found between the  $IC_{50}$  values of hybrids with 2 and 3 methylene chains ( $n = 0, 1$ ), that difference drastically increases for the longest chain length ( $n = 2$ ). The docking molecular simulations give support to this activity decrease, indicating that for hybrids with longer chain length, ( $n = 2$ ) the interaction of the BIM moiety with the peripheral active site (PAS) decreases namely due to lower  $\pi-\pi$  interaction with the aromatic residues (e.g. Trp279 and Tyr 70). Furthermore, these results showed that the introduction of a hydroxyl group in the three-methylene linker (**12a**) improved the enzyme activity ( $IC_{50} = 16.8$  nM), as compared with the

corresponding non-substituted analogue **11b** ( $IC_{50} = 30.9$  nM). Molecular simulations suggested that this improvement in the inhibitory activity can be due to an extra H-bond interaction between the hydroxyl proton and an amino acid residue (Tyr121) of the enzyme active site (see Fig 2-C). Compound **12b** presents inhibitory activity ( $IC_{50} = 18.1$  nM) in the same range of compound **12a**, although some decrease would be expected due to the chloride substitution. To compare the core moiety effect, an assay was also performed for the hydroxyphenylbenzimidazole (BIM) but this moiety showed no inhibitory activity. Hence the coupling of these two moieties brought up hybrids with very interesting capacity as AChE inhibitors. This can be attributed to strong dual-binding mode of the hybrids with both CAS and PAS of AChE, specifically due to the BIM-PAS  $\pi$ - $\pi$  interaction, although the hydroxyl substitution can also enable extra H-bond interactions within the active site and reinforce inhibition activity. Altogether the newly synthesized TAC-BIM hybrids appear as promising anti-AD compounds, acting as good AChE inhibitors.

### 2.3.2. Inhibition of self-mediated and Cu(II)-induced $A\beta_{42}$ aggregation

To test the anti-amyloidogenic activity of these novel hybrid compounds, the experimental approach relied on *in vitro* assays with ThT to monitor and quantify the aggregation of the  $A\beta_{42}$  synthetic peptide into fibrils. ThT is a histochemical dye that is known to bind to the peptide  $\beta$ -sheet conformation, which is the predominant secondary structure of amyloid-beta fibrils. The presence of fibrils can be monitored by the fluorescence emission of ThT, with the excitation and emission peaks at 446 nm and 485 nm, respectively [31,32].

The inhibition studies were carried out upon incubating  $A\beta_{42}$  in the presence and absence of the ligands. The results, depicted in **Table 1**, demonstrated that all compounds induced a decrease of the ThT fluorescence associated with the  $A\beta$  fibril binding, hence evidencing an inhibition of the  $A\beta_{42}$  self-aggregation process. In general all of them revealed good aggregation inhibitory capacity. Compounds **11b** and **12a** presented the highest inhibitory

activity (74.6% and 70.9% respectively) against fibril formation, while compounds **11(c,e,f)** presented also good activity (50.8-57.4%). In the case of compound **11d**, Table 1 presents values for the inhibition of A $\beta$  aggregation in the presence of a lower ligand concentration (40  $\mu$ M) due to the low solubility of **11d** in the phosphate buffer medium. Comparison of the activity of the tested compounds with that measured for tacrine (20%), under the same experimental conditions, clearly showed that the incorporation of the BIM moiety must be the rationale for the enhancement of their inhibitory activity in relation to tacrine. Among the hybrids studied herein, the chloro substitution resulted on the decrease of the interaction with A $\beta$ , but also noticeable change with chain length was observed. In fact, the compounds with  $n = 1$  (three methylene linkers) showed better inhibitory capacity against A $\beta_{42}$  fibril aggregation than those with shorter linker ( $n = 0$ ), but a longer chain length seems to have variable impact on the inhibitory activity: lower value for **11c** (without chloro) but higher inhibitory activity for **11f** (with chloro substitution).

An investigation of the effect of a selection of compounds on the inhibition of Cu(II)-induced A $\beta$  aggregation was also performed. In fact, these ligands possess *N,O*-donor atoms at the BIM moiety, with capacity to form 6-membered-ring metal chelates, and were found to be good Cu(II) chelators (e.g.  $pCu = 12$  for **11e** at pH 7.4) [33]. This means that the conditional dissociation constant ( $K'_d$ ) calculated for the copper(II)-**11e** complex at pH 7.4 is 10 picomolar, which is still inside the range of values ( $K'_d = 1-10$  picomolar) corresponding to compounds able to retrieve copper(II) from A $\beta$  peptide ( $K'_d = 10$  picomolar – 100 nanomolar for Cu(A $\beta$ ) complexes) [34]. Therefore, some competition for copper(II) is expected to occur between the herein studied compounds and A $\beta$  peptide and thus a concomitant interference of these ligands on the Cu-induced A $\beta$  aggregation (see Table 1). Since Zn(II) ions are present in higher quantity than Cu(II) ions in the synaptic branches, they can avoid the removal of Cu(II) by the chelators unless the ligands have higher Cu(II) over Zn(II) selectivity than the A $\beta$

peptide (4.2 for A $\beta$ <sub>16</sub> [35]), which is the case for the present chelators (e.g. selectivity of **11e** is 5.6 [33]).

The results presented in Table 1 reveal that most of the compounds induce an increase on the inhibition of Cu-induced A $\beta$  aggregation, as compared to their corresponding capacity for inhibition of self-induced A $\beta$  aggregation. Nevertheless, quantitative analysis based on fluorescence of copper(II) containing solutions may result in erroneous conclusions due to some potential quenching of the emission by this paramagnetic ion. So, a study based on a fluorescence-independent method, namely transmission electron microscopy (TEM) technique, was also performed to aid the rationalization of the results. The TEM images, depicted in Fig. 3, show that, in the presence of compound **11b**, the A $\beta$  aggregates become sparser; they also show a change on the fibril morphology to more elongated forms, especially in the absence of copper. Concerning compound **11e**, already performed TEM assays also revealed a decrease in A $\beta$  aggregates in the presence of this ligand, although somehow more elongated aggregates are shown when copper is present [33]. So, TEM seems to confirm the role of these hybrids (with or without chloro substitution in the tacrine moiety) on the inhibition of A $\beta$  aggregation both in the absence and presence of copper.

### 2.3.3. Radical scavenging activity

A selection of the novel TAC-BIM hybrids (**11b**, **11e** and **12a**) was screened for their radical scavenging capacity (antioxidant activity) based on their interaction with the 2,2-diphenyl-1-picrylhydrazyl (DPPH) free radical [36]. Analysis of the data obtained indicated a moderate radical scavenging activity ( $EC_{50} \geq 500 \mu\text{M}$ ), which is below the expected value with the BIM moiety, based on the activity of the reference moiety, hydroxyphenylbenzimidazole acid (BIMPhOH,  $EC_{50} = 160 \mu\text{M}$ ). The radical scavenging activity appeared also slightly increased with the inclusion of a hydroxyl substituent in the linker (e.g. **12a**;  $EC_{50} = 564 \mu\text{M}$ ). Overall,

the moderate radical scavenging activity presented by the TAC-BIM hybrids may be attributed to the presence of the TAC moiety ( $EC_{50} \geq 1000 \mu\text{M}$ ).

#### 2.3.4. Cell viability and neuroprotection

To evaluate the potential neuroprotective effect of the TAC-BIM hybrids (**11d**, **11e**, **11f**, **12a** and **12b**) against oxidative damage and  $A\beta$ -induced toxicity, SH-SY5Y cells were exposed to  $A\beta_{42}$  peptide or ferrous sulfate (Fe) together with L-AscH(-) (ascorbic acid, AscH(-)) in the presence and absence of these hybrid compounds. For each compound, the higher non-toxic concentration was first assessed (Fig. 4). Alzheimer's disease is pathologically characterized by the presence of extracellular neuritic plaques composed of insoluble amyloid  $\beta$  peptides [37]. Moreover, oxidative damage driven by mitochondrial impairment is also a prominent aspect of AD [38]. Interestingly, several studies reported that mitochondrial dysfunction and oxidative damage occurs in the AD brain before the onset of  $A\beta$  pathology [39].  $A\beta$  peptide forms oligomers and fibrils which are believed to influence neurodegeneration in AD. In fact,  $A\beta$  induced a decrease in SH-SY5Y cell proliferation (Fig. 5). Our results evidenced that all the tested hybrid compounds, except **11d** prevented from  $A\beta$ -induced cell toxicity, although the best protection was obtained for compounds **11e** and **11b** (Fig. 5). Interestingly, among the tested compounds **11d** presented the lowest capacity to interact with  $A\beta$  peptide (see **Table 1**). The combination of Fe and AscH(-) was herein used to induce oxidative stress. As expected, the combined Fe/AscH(-) treatment induced a decrease in cell proliferation in SHSY-5Y cells (Fig. 6). All studied TAC-BIM hybrids showed good capacity for preventing Fe/AscH(-) -mediated toxicity, although **11d** and **12b** were the most effective. In fact, all the compounds presented moderate-weak capacity to scavenge the DPPH radical, attributed to the phenol group. Indeed, Fe/AscH(-)-induced radical production (hydroxyl radical by the Fenton reaction) damages proteins, lipids and DNA, so it is possible that hybrid compounds **11d** and **12b** are more effective in preventing the formation of

different oxidative products than the radicals detected by DPPH assay. Our results highlight the relevance of multi-targeted anti-neurodegenerative drugs, like TAC-BIM hybrids, that show capacity for the radical scavenging and the inhibition of A $\beta$  oligomerization.

#### 2.4. Pharmacokinetic properties

To endeavor the drug-likeness of the novel compounds and their potential to penetrate important membranes such as the blood–brain barrier (BBB), some indicators of their pharmacokinetic profiles were predicted using QikProp program, v. 2.5 [40]. Parameters such as the calculated octanol–water partition coefficient ( $clog P$ ), the ability to cross the BBB ( $log BB$ ), the capacity to be absorbed through the intestinal tract to the blood (Caco-2 cell permeability) and the verification of Lipinski’s rule of five, may give an idea of their drug-likeness for being orally active as anti-AD agents.

As observed in **Table 2**, most of the compounds showed  $clog P$  values as recommended by Lipinski’s rule ( $\leq 5.6$ ), except compounds **11e** and **11f**. Nevertheless, almost all the compounds have a high molecular weight ( $\geq 500$  g/mol) and may have problems to be absorbed through the intestinal tract to the blood, since they have low Caco-2 permeability constants but one compound (**11e**,  $>500$  nm/s). All these hybrids present good BBB permeability ( $log BB$ ), indicating that the compounds are eligible as drug candidates for oral administration, one of these hybrids (**11a**) having zero violations while the rest has one to two violations of Lipinski’s rule [41].

### 3. Conclusions

Based on a multitarget anti-AD drug design strategy, a novel series of tacrine-hydroxyphenylbenzimidazole (TAC-BIM) hybrid compounds were developed and assessed for their biological properties including: the inhibition of AChE and of self-/Cu-induced A $\beta$  aggregation, antioxidant activity and cell neuroprotection against AD stressors. The synthesized TAC-BIM hybrids showed excellent activity (nano molar range) as AChE

inhibitors, with improved activity as compared with standard drug tacrine. Remarkably, compound **11d** showed the highest AChE inhibition ( $IC_{50} = 6.3$  nM). Regarding the inhibition of self-induced- or Cu-induced A $\beta$  aggregation, compounds with a three-methylene linker between the two main moieties ( $n = 1$ ; **11b**, **12a**) showed the highest capacity ( $IC_{50} = 74.6\%$  and  $70.9\%$  respectively). Furthermore, these compounds exhibited moderate antioxidant (radical scavenging) capacity but the best activity was found for **12a**, which includes a hydroxyl group in the linker. The compounds tend to inhibit the neurotoxicity induced by A $\beta$  and Fe/AscH(-), but **11e** and **12b** showed improved neuroprotective capacity induced by A $\beta$ , while **11d** and **12b** were the most effective against the neurotoxicity induced by the Fe/AscH(-). Overall, this newly developed series of hybrid compounds demonstrated a promising multifunctional activity, because besides the important improvement of AChE inhibitory activity, as compared with tacrine, they demonstrated further capacities for the successful addressing of some of the most important AD targets. So, these hybridization strategy revealed successful and some compounds are worthy of further developments as potential multifunctional drug candidates for AD therapy.

## 4. Experimental part

### 4.1. Chemistry

#### *General methods and materials*

Analytical grade reagents were purchased from Sigma-Aldrich, Fluka and Acros, and were used as supplied. Solvents were dried according to standard methods. The chemical reactions were monitored by TLC using alumina plates coated with silica gel 60 F<sub>254</sub> (Merck). Column chromatography separations were performed on silica gel Merck 230-400 mesh (Geduran Si 60). The melting points (m.p.) were measured with a Leica Galen III hot stage apparatus and are uncorrected. The <sup>1</sup>H and <sup>13</sup>C NMR spectra were recorded on Bruker AVANCE III spectrometers at 300 and 400 MHz, respectively. Chemical shifts ( $\delta$ ) are reported in ppm from the standard internal reference tetramethylsilane (TMS). The following abbreviations are used: s = singlet, d = doublet, t = triplet, m = multiplet. Mass spectra (ESI-MS) were performed on a 500 MS LC Ion Trap (Varian Inc., Palo Alto, CA, USA) mass spectrometer equipped with an ESI ion source, operated in the positive ion mode. For the target compounds, the elemental

analyses were performed on a Fisons EA1108 CHNS/O instrument and were within the limit of  $\pm 0.4\%$ . The electronic spectra were recorded with a Perkin Elmer Lambda 35 spectrophotometer, using thermostated 1 cm path length cells. The  $^1\text{H}$  NMR and  $^{13}\text{C}$  NMR spectra of the final compounds are presented as supplementary material (Fig. 4-11S)

#### 4.1.2. Preparation of 9-chloro-1,2,3,4-tetrahydroacridine compounds 3(a, b)

To a mixture of anthranilic acid **1(a, b)** (1 mole) and cyclohexanone (**2**) (1.2 mol) was carefully added  $\text{POCl}_3$  (25 mL) in an ice bath. The mixture was heated under reflux for 3 h, then cooled at room temperature, and concentrated to give slurry. The residue was diluted with EtOAc, neutralized with  $\text{K}_2\text{CO}_3$  aqueous solution, and washed with brine. The organic layer was dried over anhydrous  $\text{Na}_2\text{SO}_4$  and concentrated *in vacuo* to furnish a pale brown solid. It was purified by column chromatography using eluent  $\text{CH}_2\text{Cl}_2/\text{MeOH}$  (100/5) to give **3(a, b)**.

##### 4.1.2.1. 9-Chloro-1,2,3,4-tetrahydroacridine (3a)

Anthranilic acid and cyclohexanone afforded the pure title product as a dark brown solid; yield 91%; m.p. 66-68 °C;  $^1\text{H}$  NMR (300 MHz,  $\text{CDCl}_3$ )  $\delta$ : 8.14 (d,  $J = 8.4$  Hz, 1H, TAC-H-1), 7.96 (d,  $J = 8.3$  Hz, 1H, TAC-H-6), 7.67-7.62 (m, 1H, TAC-H-7), 7.53-7.48 (m, 1H, TAC-H-8), 3.11 (br, 2H, TAC-H-14), 2.98 (br, 2H, TAC-H-15), 1.94-1.90 (m, 4H, TAC-H-17); MS-ESI ( $m/z$ ): 218 ( $\text{M}^+$ ), 219 ( $\text{M}+1$ )<sup>+</sup>, 220 ( $\text{M}+2$ )<sup>+</sup>.

##### 4.1.2.2. 6,9-Dichloro-1,2,3,4-tetrahydroacridine (3b)

2-Amino-4-chloro-benzoic acid and cyclohexanone was made react, according to previously described [39], affording the pure title product as a brown solid; yield 90%; m.p. 65-67 °C;  $^1\text{H}$  NMR ( $\text{CDCl}_3$ )  $\delta$ : 8.06 (d,  $J = 8.8$  Hz, 1H TAC-1), 7.95 (d,  $J = 2.0$  Hz, 1H, TAC-H-6), 7.45 (dd,  $J = 7.0$  Hz, 2.0 Hz, 1H, TAC-H-8), 3.08 (br, 2H, TAC-H-14), 2.98 (br, 2H, TAC-H-15), 1.94 (m, 4H, TAC-H-17); MS-ESI ( $m/z$ ): 252 ( $\text{M}^+$ ), 253 ( $\text{M}+1$ )<sup>+</sup>, 254 ( $\text{M}+2$ )<sup>+</sup>.

#### 4.1.3. General Procedure for the synthesis of N-(1,2,3,4-tetrahydroacridine-9-ylamino) amine 6(a-f) and 7 (a-b)

To a mixture of **(3)** (1 eq), and different aliphatic diamines (1,2-diaminoethane, 1,3-diaminopropane, 1,4-diaminobutane **4(a-f)** and also 1,3-diaminopropan-2-ol) **5a** (2.5 eq), phenol (0.5 eq) and a catalytic amount of KI were added. The mixture is heated at 180 °C for 35 min, with completion of the reaction monitored by TLC. Then, the mixture was cooled to room temperature, treated with 5% NaOH solution, extracted with ethyl acetate and finally washed with water and brine. The organic layer was dried over anhydrous Na<sub>2</sub>SO<sub>4</sub> and concentrated under reduced pressure to give the crude product. Purification was performed by column chromatography, eluent: CH<sub>2</sub>Cl<sub>2</sub>/MeOH: 5-8%, 25%NH<sub>3</sub> per 1L.

#### 4.1.3.1. *N*-(1,2,3,4-tetrahydroacridin-9-yl)ethane-1,2-diamine (**6a**)

9-Chloro-1,2,3,4-tetrahydroacridine (**3a**) and 1,2-diaminoethane (**4a**) afforded the pure title product as a brown colour semisolid; yield 55%; <sup>1</sup>H NMR (CDCl<sub>3</sub>) δ: 8.02-7.88 (m, 2H, TAC-H-1 & H-6), 7.54 (t, *J* = 7.5 Hz, 1H, TAC-H-7), 7.34 (t, *J* = 7.6 Hz, 1H, TAC-H-8), 3.53 (t, *J* = 5.6 Hz, 2H, alkylamine-H-12), 3.07 (br, 2H, alkylamine-H-13), 2.96 (t, *J* = 5.6 Hz, 2H, TAC-H-14), 2.76 (br, 2H, TAC-H-15), 1.92-1.87 (m, 4H, TAC-H-17); MS-ESI (*m/z*): 242 (M+1)<sup>+</sup>, 243 (M+2)<sup>+</sup>.

#### 4.1.3.2. *N*-(1,2,3,4-tetrahydroacridin-9-yl)propane-1,3-diamine (**6b**)

9-Chloro-1,2,3,4-tetrahydroacridine (**3a**) and 1,3-diaminopropane (**4b**) afforded the pure title product as a brown semisolid; yield 58%; <sup>1</sup>H NMR (CDCl<sub>3</sub>) δ: 7.97 (d, *J* = 8.4 Hz, 1H, TAC-H-1), 7.89 (d, *J* = 8.4 Hz, 1H, TAC-H-6), 7.54-7.48 (m, 1H, TAC-H-7), 7.32-7.26 (m, 1H, TAC-H-8), 3.59 (t, *J* = 6.4 Hz, 2H, alkylamine-H-12), 3.03 (br, 2H, alkylamine-H-13), 2.87 (t, *J* = 6.4 Hz, 2H, TAC-H-14), 2.68 (br, 2H, TAc-H-15), 1.77-1.49 (m, 4H, alkylamine-H-16), 1.81-1.72 (m, 2H, TAC-H-17); MS-ESI (*m/z*): 256 (M+1)<sup>+</sup>, 257 (M+2)<sup>+</sup>.

#### 4.1.3.3. *N*-(1,2,3,4-tetrahydroacridin-9-yl)butane-1,4-diamine (**6c**)

9-Chloro-1,2,3,4-tetrahydroacridine (**3a**) and 1,4-diaminobutane (**4c**) afforded the pure title product as a brown colour semisolid; yield 59%;  $^1\text{H NMR}$  ( $\text{CDCl}_3$ )  $\delta$ : 7.93-7.86 (m, 2H, TAC-H-1 & H-6), 7.53-7.47 (m, 1H, TAC-H-7), 7.32-7.26 (m, 1H, TAC-H-8), 3.44 (t,  $J = 7.0$  Hz, 2H, alkylamine-H-12), 3.01 (br, 2H, alkylamine-H-13), 2.71-2.65 (m, 4H, TAC-14 & H-15), 1.88-1.85 (m, 4H, TAC-H-17), 1.68-1.60 (m, 2H, alkylamine-H-16), 1.54-1.44 (m, 2H, alkylamine-H-18); MS-ESI ( $m/z$ ): 270 ( $\text{M}+1$ ) $^+$ , 271 ( $\text{M}+2$ ) $^+$ .

#### 4.1.3.4. *N*-(6-chloro-1,2,3,4-tetrahydroacridin-9-yl)ethane-1,2-diamine (**6d**)

6,9-Dichloro-1,2,3,4-tetrahydroacridine (**3b**) and 1,2-diaminoethane (**4d**) afforded the pure title product as a brown solid semi-solid; yield 60%;  $^1\text{H NMR}$  ( $\text{CDCl}_3$ )  $\delta$ : 7.85-7.79 (m, 2H, TAC-H-1 & H-6), 7.15 (d,  $J = 7.1$ , 1H, TAC-H-8), 3.40-3.34 (m, 2H, alkylamine-H-12), 2.93 (br, 2H, TAC-H-14), 2.96 (t,  $J = 5.7$  Hz, 2H, alkylamine-H-13), 2.63 (br, 2H, TAC-H-15), 1.84-1.79 (m, 4H, TAC-H-17); MS-ESI ( $m/z$ ): 276 ( $\text{M}$ ) $^+$ , 277 ( $\text{M}+1$ ) $^+$ , 278 ( $\text{M}+2$ ) $^+$ .

#### 4.1.3.5. *N*-(6-chloro-1,2,3,4-tetrahydroacridin-9-yl)propane-1,3-diamine (**6e**)

6,9-Dichloro-1,2,3,4-tetrahydroacridine (**3b**) and 1,3-diaminopropane (**4e**) afforded the pure title product as a brown semi-solid; yield 62%;  $^1\text{H NMR}$  ( $\text{CDCl}_3$ )  $\delta$ : 7.93-7.85 (m, 2H, TAC-H-1 & H-6), 7.15 (d,  $J = 7.1$  Hz, 1H, TAC-H-8), 3.60 (t,  $J = 6.5$  Hz, 2H, alkylamine-H-12), 3.0 (br, 2H, TAC-H-14), 2.90 (t,  $J = 6.3$  Hz, 2H, alkylamine-H-13), 2.66 (br, 2H, TAC-H-15), 1.90-1.87 (m, 4H, TAC-H-17), 1.81-1.74 (m, 2H, alkylamine-H-16); MS-ESI ( $m/z$ ): 290 ( $\text{M}$ ) $^+$ , 291 ( $\text{M}+1$ ) $^+$ , 292 ( $\text{M}+2$ ) $^+$ , 293 ( $\text{M}+3$ ) $^+$ .

#### 4.1.3.5. *N*-(6-chloro-1,2,3,4-tetrahydroacridin-9-yl)propane-1,4-diamine (**6f**)

6,9-Dichloro-1,2,3,4-tetrahydroacridine (**3b**) and 1,4-diaminobutane (**4f**) afforded the pure title product as a brown semi-solid; yield 61%;  $^1\text{H NMR}$  ( $\text{CDCl}_3$ )  $\delta$ : 7.87-7.85 (m, 2H, TAC-H-1 & H-6), 7.22 (d,  $J = 6.9$  Hz, 1H, TAC-H-8), 3.46 (t,  $J = 7.1$  Hz, 2H, alkylamine-H-12), 2.99 (br, 2H, TAC-H-14), 2.71 (t,  $J = 6.9$  Hz, 2H, alkylamine-H-13), 2.63 (br, 2H, TAC-H-

15), 1.89-1.86 (m, 4H, TAC-H-17), 1.71-1.64 (m, 2H,alkylamine-H-16), 1.54-1.47 (m, 2H, alkylamine-H-18); MS-ESI ( $m/z$ ): 304 ( $M^+$ ), 305 ( $M+1$ )<sup>+</sup>, 306 ( $M+2$ )<sup>+</sup>.

#### 4.1.3.6. 1-Amino-3-((1,2,3,4-tetrahydroacridin-9-yl)amino)propan-2-ol (7a)

9-Chloro-1,2,3,4-tetrahydroacridine (**3a**) and 1,3-diaminopropan-2-ol (**5**) afforded the pure title product as a brown solid; yield 60%; m.p. 90-92 °C; MS-ESI ( $m/z$ ):270 ( $M-1$ )<sup>+</sup>, 271 ( $M$ )<sup>+</sup>, 272 ( $M+1$ )<sup>+</sup>.

#### 4.1.3.7 1-Amino-3-((6-chloro-1,2,3,4-tetrahydroacridin-9-yl)amino)propan-2-ol (7b)

6,9-Dichloro-1,2,3,4-tetrahydroacridine (**3b**) and 1,3-diaminopropan-2-ol (**5**) afforded the pure title product as a light brown solid; yield 65%; m.p.89-90°C; MS-ESI ( $m/z$ ): 304 ( $M-1$ )<sup>+</sup>, 305 ( $M$ )<sup>+</sup>, 306 ( $M+1$ )<sup>+</sup>.

#### 4.1.4. 2-(2-Hydroxyphenyl)-1H-benzoimidazole-6-carboxylic acid (10)

To a solution of aldehyde (**9**) (2 mmol) in 6.5 mL of *N,N*-dimethyl acetamide were added 3,4-diaminobenzoic acid (**8**) (2 mmol) and Na<sub>2</sub>S<sub>2</sub>O<sub>5</sub> (2.4 mmol). The mixture was heated to 100 °C for 7-12 h until the completion of reaction confirmed by TLC. The reaction mixture was then cooled, diluted with ethyl acetate, dried (MgSO<sub>4</sub>) and concentrated in *vacuo*. The solid obtained was collected on a sintered-glass filter and washed with dichloromethane to provide the desired compound **10** as yellow color [26]; yield 62%; m.p. >300 °C. <sup>1</sup>H NMR (400 MHz, DMSO-d<sub>6</sub>) δ: 8.25 (s, 1H, BIM-H-2) , 8.10 (d, *J* = 8 Hz, 1H, BIM-H-3), 7.91 (d, *J* = 8 Hz, 1H, BIM-H-4), 7.73 (d, *J* = 8 Hz, 1H, BIM-H-5), 7.41 (t, *J* = 8 Hz, 1H, BIM-H-9), 7.05 (dd, *J* = 8 Hz, 2H, H-10 & H-11). <sup>13</sup>C NMR (400 MHz, DMSO-d<sub>6</sub>) δ: 168.10, 158.46, 132.70, 127.24, 125.74, 124.55, 119.75, 117.73, 112.95; MS-ESI ( $m/z$ ): 253 ( $M-1$ )<sup>+</sup>, 254 ( $M$ )<sup>+</sup>, 255 ( $M+1$ )<sup>+</sup>.

#### 4.1.5. General procedure for synthesis of 2-(2-hydroxyphenyl)-*N*-(3-((1,2,3,4-tetrahydroacridin-9-yl)amino)yl)-1H-benzoimidazole-6-carboxamide 9(a-f) and 10 (a-b)

To a solution of hydroxyphenylbenzimidazole carboxylic acid (**10**) (1 eq 100 mg) in anhydrous DMF (5 mL), tacrine-alkylamine, **6(a-f)** and **7(a,b)**, DCC and *N*-hydroxysuccinimide were added and the mixture was stirred at room temperature under

nitrogen atmosphere for two days, until completion of the reaction, monitored by TLC. The formed *N,N*-dicyclohexylurea (DCU) precipitate was filtered off and DMF was evaporated under vacuum. The solid compound obtained was further purified through column chromatography (7 to 15% CH<sub>2</sub>Cl<sub>2</sub>:MeOH and 2% NH<sub>3</sub>).

4.1.5.1. *2-(2-Hydroxyphenyl)-N-(2-((1,2,3,4-tetrahydroacridin-9-yl)amino)ethyl)-1H-benzoimidazole-6-carboxamide (11a)*

*N*-(1,2,3,4-tetrahydroacridin-9-yl)ethane-1,2-diamine (**6a**) and 2-(2-hydroxyphenyl)-1H-benzoimidazole-6-carboxylic acid (**10**) afforded the pure title product as a light yellow color solid; yield 24%; m.p. 205-207 °C; <sup>1</sup>H NMR (400 MHz, DMSO-d<sub>6</sub>) δ: 8.56 (d, *J* = 8 Hz, 1H, TAC-H-1), 8.17 (m, 3H, BIM-H-2, H-3 & H-4), 7.85 (t, *J* = 8 Hz, 1H, TAC-H-5), 7.58 (t, *J* = 8 Hz, 1H, BIM-H-6), 7.40 (m, 2H, TAC-H-7 & H-8), 7.22 (s, 1H, BIM-H-9), 7.03 (dd, 2H, BIM-H-10 & H-11), 4.12 (s, 2H, alkylamine-H-12), 3.89 (s, 2H, alkylamine-H-13), 2.95 (s, 2H, TAC-H-14), 2.73 (s, 2H, TAC-H-15), 1.80 (s, 4H, TAC-H-17); MS-ESI (m/z): 476 (M-1)<sup>+</sup>, 477 (M)<sup>+</sup>, 478 (M+1)<sup>+</sup>; elemental analysis calcd. for C<sub>29</sub>H<sub>27</sub>N<sub>5</sub>O<sub>2</sub> · 1H<sub>2</sub>O · 1 MeOH: C 71.58, H 5.62, N 13.12%; found: C 71.65, H 5.65, N 13.50%.

4.1.5.2. *2-(2-Hydroxyphenyl)-N-(3-((1,2,3,4-tetrahydroacridin-9-yl)amino)propyl)-1H-benzoimidazole-5-carboxamide (11b)*

*N*-(1,2,3,4-tetrahydroacridin-9-yl)propane-1,3-diamine (**6b**) and 2-(2-hydroxyphenyl)-1H-benzoimidazole-6-carboxylic acid (**10**) afforded the pure title product as light yellow color solid; yield 42%; m.p. 193-195 °C; <sup>1</sup>H NMR (400 MHz, DMSO-d<sub>6</sub>) δ: 8.48 (s, 1H, TAC-H-1), 8.21 (s, 2H, BIM-H-2 & H-3), 7.87 (m, 5H, BIM-H-4, H-5, TAC-H-6, H-7 & H-8), 7.69 (s, 1H, BIM-H-9), 7.51 (d, *J* = 8 Hz, 2H, H-10 & H-11), 4.02 (s, 2H, alkylamine-H-12), 3.48 (s, 2H, alkylamine-H-13), 3.00 (s, 2H, alkylamine-H-14), 2.73 (s, 2H, alkylamine-H-15), 2.08 (s, 2H, alkylamine-H-16), 1.83 (s, 4H, TAC-H-17). <sup>13</sup>C NMR (400 MHz, DMSO-d<sub>6</sub>) δ: 167.23,

158.45, 156.20, 150.95, 138.44, 133.02, 132.63, 127.15, 125.51, 125.43, 119.75, 119.65, 117.70, 115.99, 112.94, 111.72, 45.43, 30.47, 29.41, 24.35, 21.87, 20.89. MS-ESI (m/z): 490 (M-1)<sup>+</sup>, 491 (M)<sup>+</sup>, 492 (M+1)<sup>+</sup>; elemental analysis calcd. for C<sub>30</sub>H<sub>29</sub>N<sub>5</sub>O<sub>2</sub>·1.8·CH<sub>2</sub>Cl<sub>2</sub>: C 62.62, H 5.10, N 10.87%; found: C 62.40, H 5.28, N 11.77%.

4.1.5.3. *2-(2-Hydroxyphenyl)-N-(4-((1,2,3,4-tetrahydroacridin-9-yl)amino)butyl)-1H-benzoimidazole-5-carboxamide (11c)*

*N*-(1,2,3,4-tetrahydroacridin-9-yl)butane-1,4-diamine (**6c**) and 2-(2-hydroxyphenyl)-1H-benzoimidazole-6-carboxylic acid (**10**) afforded the pure title product as light yellow color compound; yield 45%; m.p. 174-176 °C; <sup>1</sup>H NMR (400 MHz, DMSO-d<sub>6</sub>) δ: 8.50 (s, TAC-H-1), 8.12 (s, 3H, BIM-H-2 & H-3, NH-proton), 7.78 (s, 1H, BIM-H-4), 7.70 (s, 2H, & H-5, TAC-H-6), 7.53 (s, 1H, TAC-H-7), 7.37 (m, 2H, TAC-H-8 & H-9), 7.05 (s, 1H, BIM-H-10 & H-11), 5.63 (brs, 1H, OH-proton), 3.48 (s, alkylamine-H-12), 3.29 (s, 2H, alkylamine-H-13), 2.88 (s, 2H, TAC-H-14), 2.70 (s, 2H, TAC-H-15), 1.78 (s, 4H, TAC-H-17), 1.62 (s, 4H, alkylamine-H-18 & H-19). <sup>13</sup>C NMR (400 MHz, DMSO-d<sub>6</sub>) δ: 166.81, 158.51, 157.72, 153.78, 151.25, 146.56, 132.56, 129.90, 128.74, 127.91, 127.03, 123.85, 123.69, 122.77, 120.31, 119.71, 117.72, 115.91, 113.01, 48.18, 33.46, 28.53, 27.08, 25.47, 23.09, 22.68. MS-ESI (m/z): 504 (M-1)<sup>+</sup>, 505 (M)<sup>+</sup>, 506 (M+1)<sup>+</sup>; elemental analysis calcd. for C<sub>30</sub>H<sub>29</sub>N<sub>5</sub>O<sub>2</sub>·1·MeOH: C 69.04, H 5.97, N 12.92%; found: C 69.03, H 6.12, N 13.11%.

4.1.5.4. *N-(2-((6-chloro-1,2,3,4-tetrahydroacridin-9-yl)amino)ethyl)-2-(2-hydroxyphenyl)-1H-benzoimidazole-6-carboxamide (11d)*

*N*-(6-chloro-1,2,3,4-tetrahydroacridin-9-yl)ethane-1,2-diamine (**6d**) and 2-(2-hydroxyphenyl)-1H-benzoimidazole-6-carboxylic acid (**10**) afforded the pure title product as cream color solid; yield 35%; m.p. 178-180 °C; <sup>1</sup>H NMR (400 MHz, DMSO-d<sub>6</sub>) δ: 8.69 (s, 1H, TAC-H-1), 8.23 (s, 3H, BIM-H-2, H-3 & H-4), 7.72 (s, 3H, BIM-H-5, TAC-amide-NH, TAC-H-7), 7.37 (d, J

= 8 Hz, 2H, TAC-H-8 & BIM-H-9), 7.05 (s, 2H, Bim-H-10 & H-11), 6.05 (s, 1H, BIM-NH), 3.73 (s, 2H, alkylamine-H-12), 3.56 (s, 2H, alkylamine-H-13), 2.85 (s, 2H, TAC-H-14), 2.71 (s, 2H, TAC-H-15), 1.76 (s, 4H, TAC-H-17).  $^{13}\text{C}$  NMR (400 MHz, DMSO- $d_6$ )  $\delta$ : 167.29, 158.33, 158.05, 153.38, 151.13, 146.80, 132.97, 132.16, 128.96, 126.63, 125.82, 125.70, 123.61, 122.43, 119.27, 117.97, 117.28, 115.48, 112.49, 48.03, 40.43, 32.90, 24.80, 22.43, 22.03. MS-ESI (m/z): 510 (M-1) $^+$ , 511 (M) $^+$ , 512 (M+1) $^+$ ; elemental analysis calcd. for  $\text{C}_{29}\text{H}_{26}\text{ClN}_5\text{O}_2 \cdot 2 \cdot \text{H}_2\text{O} \cdot 1 \cdot \text{MeOH}$ : C 62.12, H 5.91, N 12.07%; found: C 61.83, H 5.66, N 11.93%.

4.1.5.5. *N*-(3-((6-chloro-1,2,3,4-tetrahydroacridin-9-yl)amino)propyl)-2-(2-hydroxyphenyl)-1H-benzoimidazole-5-carboxamide (**11e**)

*N*-(6-chloro-1,2,3,4-tetrahydroacridin-9-yl)propane-1,3-diamine (**6e**) and 2-(2-hydroxyphenyl)-1H-benzoimidazole-6-carboxylic acid (**10**) afforded the pure title product as cream color compound; yield 63%; m.p. 179-181 °C;  $^1\text{H}$  NMR (400 MHz, MeOD)  $\delta$ : 8.13 (d,  $J$  = 8 Hz, 1H, TAC-H-1), 8.05 (brs, 1H, NH-proton), 7.92 (d,  $J$  = 8 Hz, 1H, BIM-H-2), 7.70 (d,  $J$  = 8 Hz, 1H, BIM-H-3), 7.61 (d,  $J$  = 8 Hz, 2H, BIM-H-4 & H-5), 7.35 (d,  $J$  = 8 Hz, 1H, TAC-H-6), 7.26 (d,  $J$  = 8 Hz, 1H, TAC-H-9), 6.99 (dd,  $J$  = 8 Hz, 2H, BIM-H-10 & H-11), 5.48 (s, OH proton), 3.74 (s, 2H, alkylamine-H12), 3.54 (s, 2H, alkylamine-H-13), 2.89 (s, 2.70, TAC-H-14), 2.70 (s, 2H, TAC-H-15), 2.00 (s, 2H, alkylamine-H-16), 1.85 (s, 4H, TAC-H-17).  $^{13}\text{C}$  NMR (400 MHz, DMSO- $d_6$ )  $\delta$ : 173.27, 167.12, 158.48, 15.78, 151.91, 133.86, 132.59, 127.06, 126.21, 125.33, 124.27, 119.71, 118.11, 117.71, 115.59, 112.93, 55.38, 45.61, 37.21, 32.80, 30.96, 25.69, 25.30, 22.78, 22.27. MS-ESI (m/z): 524 (M-1) $^+$ , 525 (M) $^+$ , 526 (M+1) $^+$ ; elemental analysis calcd. for  $\text{C}_{30}\text{H}_{28}\text{ClN}_5\text{O}_2 \cdot 2.67 \cdot \text{H}_2\text{O} \cdot 0.9 \text{ MeOH}$ : C 61.55, H 6.17, N 11.61%; found: C 61.28, H 5.32, N 12.09%.

4.1.5.6. *N*-(4-((6-chloro-1,2,3,4-tetrahydroacridin-9-yl)amino)butyl)-2-(2-hydroxyphenyl)-1*H*-benzoimidazole-5-carboxamide (**11f**)

*N*-(6-chloro-1,2,3,4-tetrahydroacridin-9-yl)propane-1,4-diamine (**6f**) and 2-(2-hydroxyphenyl)-1*H*-benzoimidazole-6-carboxylic acid (**10**) afforded the pure title product as cream color solid; yield 69%; m.p. 154-156 °C; <sup>1</sup>H NMR (400 MHz, DMSO-*d*<sub>6</sub>) δ: 8.45 (s, 1H, TAC-H-1), 8.14 (s, 2H, BIM-H-2 & H-3), 8.08 (brs, 1H, NH-proton), 7.78 (s, 1H, BIM-H-4), 7.69 (s, 2H, BIM-H-5 & H-6), 7.40 (s, 1H, TAC-H-8), 7.29 (s, 1H, BIM-H-9), 7.05 (s, 2H, BIM-H-10 & H-11), 5.56 (brs, 1H, OH-proton), 3.46 (s, 2H, alkylamine-H-12), 3.18 (s, 2H, alkylamine-H-13), 2.86 (s, 2H, TAC-H-14), 2.68 (s, 2H, TAC-H-15), 1.77 (s, 4H, TAC-H-17), 1.61 (s, 4H, alkylamine-H-18 & H-19). <sup>13</sup>C NMR (400 MHz, DMSO-*d*<sub>6</sub>) δ: 166.51, 159.52, 158.22, 153.46, 150.63, 147.75, 132.59, 132.55, 129.64, 126.84, 126.69, 125.60, 123.56, 119.39, 118.83, 117.42, 116.14, 112.70, 48.77, 47.91, 33.69, 28.35, 26.77, 25.17, 22.76, 22.41; MS-ESI (m/z): 539 (M-1)<sup>+</sup>, 540 (M)<sup>+</sup>, 541 (M+1)<sup>+</sup>; elemental analysis calcd. for C<sub>31</sub>H<sub>30</sub>ClN<sub>5</sub>O<sub>2</sub>·1.15MeOH: C 66.69, H 6.10, N 12.04%; found: C 66.40, H 6.12, N 12.36%.

4.1.5.7. *N*-(2-hydroxy-3-((1,2,3,4-tetrahydroacridin-9-yl)amino)propyl)-2-(2-hydroxyphenyl)-1*H*-benzoimidazole-5-carboxamide (**12a**)

1-Amino-3-((1,2,3,4-tetrahydroacridin-9-yl)amino)propan-2-ol (**7a**) and 2-(2-hydroxyphenyl)-1*H*-benzoimidazole-6-carboxylic acid (**10**) afforded the pure title product as cream color compound; yield 52%; m.p. 173-175 °C; <sup>1</sup>H NMR (400 MHz, DMSO-*d*<sub>6</sub>) δ: 8.55 (s, 1H, TAC-H-1), 8.16 (d, *J* = 8 Hz, 1H, BIM-H-2), 8.08 (d, *J* = 8 Hz, 1H, BIM-H-3), 7.80 (d, *J* = 8 Hz, 1H, BIM-H-4), 7.71 (d, *J* = 8 Hz, 2H, BIM-H-5 & TAC-H-6), 7.53 (t, *J* = 8 Hz, 1H, TAC-H-7), 7.41 (t, *J* = 8 Hz, 1H, TAC-H-8), 7.33 (t, *J* = 8 Hz, 1H, BIM-H-9), 7.05 (m, 2H, BIM-H-10 & H-11), 5.53 (brs, 1H, OH-proton), 5.31 (brs, 1H, NH-proton), 3.85 (s, 1H, alkylamine-H-16), 3.98 (s, 2H, alkylamine-H-12), 3.35 (s, 2H, 3.31, alkylamine-H-13), 2.90 (s, 2H, TAC-H-14), 2.77 (s, 2H, TAC-H-15), 1.80 (s, 4H, TAC-H-17). <sup>13</sup>C NMR (400 MHz, DMSO-*d*<sub>6</sub>) δ: 167.46,

158.50, 153.83, 151.24, 132.61, 129.63, 128.64, 128.26, 177.04, 173.70, 120.37, 123.70, 119.73, 117.74, 116.20, 112.99, 69.80, 52.23, 44.13, 33.68, 25.14, 23.12, 22.77; MS-ESI (m/z): 506 (M-1)<sup>+</sup>, 507 (M)<sup>+</sup>, 508 (M+1)<sup>+</sup>; elemental analysis calcd. for C<sub>30</sub>H<sub>28</sub>ClN<sub>5</sub>O<sub>3</sub>·1H<sub>2</sub>O·1.37 MeOH: C 66.16, H 6.46, N 12.22%; found: C 65.75, H 6.20, N 12.22%.

4.1.5.8. *N*-(3-((6-chloro-1,2,3,4-tetrahydroacridin-9-yl)amino)-2-hydroxypropyl)-2-(2-hydroxyphenyl)-1H-benzoimidazole-5-carboxamide (**12b**)

1-Amino-3-((6-chloro-1,2,3,4-tetrahydroacridin-9-yl)amino)propan-2-ol (**7b**) and 2-(2-hydroxyphenyl)-1H-benzoimidazole-6-carboxylic acid (**10**) afforded the pure title product as cream color solid; yield 73%; m.p. 258-260 °C; <sup>1</sup>H NMR (400 MHz, DMSO-d<sub>6</sub>) δ: 8.54 (s, 1H, TAC-H-1), 8.13 (dd, *J* = 8 Hz, 3H, BIM-H-2, H-3 & H-4), 7.80 (d, *J* = 8 Hz, 1H, BIM-H-5), 7.71 (s, 2H, TAC-H-6 & H-7), 7.41 (t, *J* = 8 Hz, 1H, TAC-H-8), 7.29 (d, *J* = 8 Hz, 1H, BIM-9), 7.06 (d, *J* = 8 Hz, 2H, BIM-H-10 & H-11), 3.84 (s, 1H, alkylamine-H-16), 3.59 (s, 2H, alkylamine-H-12), 3.31 (s, 2H, alkylamine-H-13), 2.88 (s, 2H, TAC-H-14), 2.75 (s, 2H, TAC-H-15), 1.79 (s, 4H, TAC-H-17). <sup>13</sup>C NMR (400 MHz, DMSO-d<sub>6</sub>) δ: 167.46, 159.78, 158.51, 153.83, 151.14, 148.08, 132.92, 132.58, 129.61, 127.17, 127.02, 125.99, 123.89, 119.71, 119.02, 117.73, 116.62, 112.99, 69.83, 52.24, 44.12, 34.00, 25.11, 23.03, 22.72; MS-ESI (m/z): 540 (M-1)<sup>+</sup>, 542 (M)<sup>+</sup>, 543 (M+1)<sup>+</sup>; elemental analysis calcd. for C<sub>30</sub>H<sub>28</sub>ClN<sub>5</sub>O<sub>3</sub>·1MeOH: C 64.86, H 5.62, N 12.20%; found: C 64.84, H 5.30, N 12.54%.

## 4.2. Molecular Modeling

To perform our docking studies, the X-ray crystallographic structure of *Torpedo californica*-AChE (*TcAChE*) complexed with an inhibitor was taken from RCSB Protein Data Bank (PDB entry 1ODC), in order to be used as receptor. This structure was chosen because of the similarity between its original inhibitor ((*N*-4'-quinolyl-*N'*-9''-(1'',2'',3'',4''-

tetrahydroacridinyl)-1,8-diaminooctane) and the herein studied ligands: all have a tacrine moiety and an aromatic group linked through an alkyl chain. The structure of original complex was treated using Maestro v. 9.3 [42] by removing the original ligand, solvent and co-crystallization molecules, and then adding the hydrogen atoms. The ligands were built using Maestro, and then, using Ghemical v. 2.0 [43], they were submitted to random conformational search (RCS) of 1000 cycles and 2500 optimization steps using Tripos 5.2 force field [44]. The optimized ligand models were docked into the active site of the AChE model structure with GOLD software v. 5.2 [45], which zone of interest was defined as the residues within 10 Å from the original position of the ligand in the crystal structure. The ‘allow early termination’ option was deactivated, and the remaining default parameters of GOLD were used. The ligands were subjected to 100 genetic algorithm steps using ASP as fitness function.

### 4.3. Acetylcholinesterase activity

The enzymatic activity of AChE (*Electrophorus electricus* (electric eel) purchased from *Sigma Aldrich*) was measured using the method previously described [46,47]. The assay solution contained 374 µL of 4-(2-hydroxyethyl)-1-piperazine-ethanesulfonic acid (HEPES) buffer solution (50 mM; pH = 8.0), a variable volume (10–50 µL) of the stock solution of each compound in methanol (1 mg/mL), 25 µL of AChE stock solution, and the necessary amount of methanol to attain 0.925 mL of the sample mixture in a 1-mL cuvette. The samples were left to incubate for 15 min, and then, 75 µL of acetyl thiocholine iodide (AChI) solution (16 mM) and 476 µL of DTNB (3 mM) were added. The reaction was monitored for 5 min at 405 nm. Assays were run with a blank containing all the components except AChE, which was replaced by HEPES buffer. The velocities of the reaction were calculated as well as the enzyme activity. A control reaction was carried out using the sample solvent (methanol) in the absence of any tested compound, and it was considered as 100% activity. The percentage of

inhibition of the enzyme activity, due to the presence of increasing test compound concentration, was calculated by the following Eq. (1),

$$\%I = 100 - (v_i/v_o \times 100) \quad (1)$$

in which  $v_i$  is the initial reaction rate in the presence of inhibitor and  $v_o$  is the initial rate of the control reaction. The inhibition curves were obtained by plotting the percentage of enzymatic inhibition versus inhibitor concentration, and a calibration curve was obtained from which the linear regression parameters were obtained.

#### 4.4. Inhibition of A $\beta$ (1–42) aggregation

The A $\beta_{42}$  samples, stored at -20 °C, were treated with 1,1,1,3,3,3-hexafluoropropan-2-ol (HFIP) to avoid self-aggregation and reserved. HFIP pretreated A $\beta_{42}$  samples were resolubilized with a CH<sub>3</sub>CN/Na<sub>2</sub>CO<sub>3</sub> (300  $\mu$ M)/NaOH (250  $\mu$ M) (48.3:48.3:4.3, v/v/v) solvent mixture in order to have a stable stock solution. This A $\beta_{42}$  alkaline solution (500  $\mu$ M) was diluted in phosphate buffer (0.215 M, pH 8.0) to obtain a 40  $\mu$ M solution. Due to the hydrophobic nature of the compounds under study, they were firstly dissolved in methanol (1 mg/mL) and then further diluted in phosphate buffer to a final concentration of 80  $\mu$ M.

To study A $\beta_{42}$  aggregation inhibition, a reported method, based on the fluorescence emission of thioflavin T (ThT), was followed [31,32,46]. Firstly, A $\beta_{42}$  (30  $\mu$ L) samples and the tested compounds (10  $\mu$ L) were diluted with phosphate buffer to a final concentration of 40  $\mu$ M (A $\beta$ ) and 80  $\mu$ M (compounds), or 40  $\mu$ M (A $\beta$ ), 40  $\mu$ M (CuCl<sub>2</sub>) and 80  $\mu$ M (compounds), and then, they were incubated for 24 h at 37 °C, without stirring. As for the control, a sample of the peptide was incubated under identical conditions but without the inhibitor. After incubation, the samples were added to a 96-well plate (BD Falcon) with 180  $\mu$ L of 5  $\mu$ M ThT in 50 mM glycine-NaOH (pH 8.5) buffer. Blank samples were prepared for each concentration in a similar way, devoid of peptide. After 5-min incubation with the dye, the ThT fluorescence was

measured using a Spectramax Gemini EM (Molecular Devices) at the following wavelengths: 446 nm (excitation) and 485 nm (emission). The percent inhibition of the self-induced aggregation due to the presence of the test compound was calculated by the Eq. (2), in which  $IF_i$  and  $IF_0$  corresponded to the fluorescence intensities, in the presence and the absence of the test compound, minus the fluorescence intensities due to the respective blanks.

$$I\% = 100 - (IF_i / IF_0 \times 100) \quad (2)$$

The reported values were obtained as the mean  $\pm$  SEM of two different experiments.

The samples for the *Transmission Electron Microscopy* (TEM) assays were previously prepared according to the following procedure. A $\beta$  stock solutions were prepared by dissolving the lyophilized peptide in a mixture of acetonitrile (48  $\mu$ L), 2% NH<sub>4</sub>OH (10  $\mu$ L) and NaCl 300  $\mu$ M (48  $\mu$ L). The peptide stock solution was diluted to a final concentration of 50  $\mu$ M in a HEPES buffered solution (50 mM, pH = 6.6). For the inhibition studies, compounds (50  $\mu$ M final concentration) were added to the sample of A $\beta$  (25  $\mu$ M final concentration) in the absence or in the presence of copper chloride (2  $\mu$ M final concentration) followed by incubation for 24 h at 37 °C.

*Transmission Electron Microscopy (TEM)*. Formvar/Carbon 200-mesh Cu grids (Ted Pella) were treated with amyloid- $\beta$  peptide aggregated samples (10  $\mu$ L) for 2 min at room temperature. Excess samples were removed using filter paper followed by washing twice with deionized water. Each grid incubated with uranyl acetate (1%, 10  $\mu$ L, 1 min) was stained and dried for 15 min at room temperature. Images from each sample were taken by a Hitachi H8100 TEM with a LaB6 filament (200kV, 10000-20000 x magnification).

#### 4.5. Radical scavenging activity

The radical scavenging activity or, more precisely, the electron and proton donation ability, was evaluated by the DPPH method previously described [36,47]. To a 2.5 mL solution of

DPPH (0.002%) in methanol, four samples of each compound in solution were added in different volumes to obtain different concentrations in a 3.5 mL final volume. The samples were incubated for 30 min at room temperature.

The absorbance was measured at 517 nm against the corresponding blank (methanol). The antioxidant activity was calculated by Eq. (3) [47].

$$\%AA = \frac{A_{DPPH} - A_{sample}}{A_{DPPH}} \quad (3)$$

The tests were carried out in triplicate. The compound concentration providing 50% of antioxidant activity ( $EC_{50}$ ) was obtained by plotting the antioxidant activity against the compound concentration.

#### 4.7. Cells and treatments

Human Neuroblastoma SH-SY5Y cell line was purchased from ATCC-CRL-2266. In short, the cells were grown in Dulbecco's modified Eagle's medium (DMEM) obtained from Gibco-Invitrogen (Life Technologies Ltd, UK) with 10% heat inactivated fetal calf serum, containing 50 U/mL penicillin and 50  $\mu$ g/mL streptomycin, under a humidified atmosphere of 95% air- 5%  $CO_2$  at 37 °C. Cells were plated at  $0.12 \times 10^6$  cells/mL for cell proliferation assay.

The tested compounds (**11d**, **11e**, **11f**, **12a** and **12b**) were dissolved in DMSO at a concentration of 25 mM and aliquots were stored at -20°C. A concentration screening (from 0.02  $\mu$ M to 10  $\mu$ M) was performed in order to choose the highest non-toxic concentration. As a result, the compounds **11d**, **11f** and **12b** were added to the medium at 1  $\mu$ M final concentration; compound **9e** was added to the medium at 0.1  $\mu$ M final concentration and **12a** at 2.5  $\mu$ M final concentration. The final concentration of DMSO in culture media did not exceed 0.05% (v/v) and no alterations on cells were observed. Cells were pre-incubated for 1 h

with the compounds and then incubated with A $\beta$ <sub>42</sub> or ferrous sulfate (Fe)/L-AscH(-) ascorbic acid (AscH(-)) for another 24 h. A $\beta$ <sub>42</sub> was prepared as 276.9  $\mu$ M stock in sterile water and added to the medium at 1  $\mu$ M final concentration. Fe was freshly prepared as 0.36 M stock in water and added to the medium at 500  $\mu$ M final concentration. AscH(-) was freshly prepared as 80 mM stock in water and added to the medium at 5 mM final concentration. A $\beta$ <sub>42</sub> was purchased from Bachem (Torrance, CA, USA) and Fe and AscH(-) from Sigma Chemical Co (St. Louis, MO, USA). For all conditions tested, control experiments were performed in which the compounds tested, A $\beta$ <sub>42</sub> or Fe/ AscH(-) were not added.

Cell reduction ability to measure cell proliferation was determined by the colorimetric MTT (3-(4,5-dimethylthiazol-2-yl)-2,5-diphenyltetrazolium bromide) assay according to the method of Mosmann [48]. Briefly, cells were incubated with 0.5 mL MTT (0.5 mg/mL) at 37 °C for 1.5 h. In viable cells, MTT is metabolized into a formazan that absorbs light at 570 nm. Afterwards, the formazan precipitates were solubilized with 0.5 mL of acidic isopropanol (0.04 M HCl/isopropanol). The absorbance was measured at 570 nm using a SpectramaxPlus 384 spectrophotometer (Molecular Devices). MTT reduction ability was expressed as a percentage of the control value obtained for untreated cells. All data result from the analysis of duplicates per experimental condition in at least three independent experiments and are expressed as the mean $\pm$ SEM. Statistical analyses were performed using GraphPad Prism 5 (GraphPad Software, San Diego, CA, USA). Statistical tests between multiple data sets and conditions were carried out using a one-way analysis of variance (ANOVA) with pairwise multiple comparison procedures using the post hoc Bonferroni's test to determine statistical significance, as appropriate. A p value <0.05 was considered statistically significant.

#### **4.8. Prediction of pharmacokinetic properties**

To analyze the potential of the new compounds as anti-AD drugs, a brief prediction on pharmacokinetic proprieties was performed *in silico*. Parameters such as the lipo-hydrophilic

character (clog  $P$ ), blood–brain barrier partition coefficient (log BB), ability to be absorbed through the intestinal tract (Caco-2 cell permeability) and CNS activity were calculated.

The ligands were built and minimized as previously mentioned for the docking studies. The structures were submitted to the calculation of these relevant pharmacokinetic proprieties and descriptors using QikProp v. 2.5 [40]. These predictions are for orally delivered drugs and assume non active transport.

**Acknowledgements.** The authors acknowledge the Portuguese *Fundação para a Ciência e Tecnologia* (FCT) for the project UID/QUI/00100/2013, and also the Portuguese NMR (IST-UL Center) and Mass Spectrometry Networks (Node IST-CTN) for providing access to their facilities. We also thank the doctoral fellowship from Erasmus Namaste program (AH).

#### References:

- [1] Alzheimer's Association, 2015 Alzheimer's disease facts and figures, *Alzheimers Dement.* 11 (2015) 332–384.
- [2] World Health Organization. Dementia, WHO fact sheet: 2016. <http://www.who.int/mediacentre/factsheets/fs362/en/>
- [3] W. Henry, H.W. Querfurth, F.M. LaFerla, Alzheimer's disease, *N. Engl. J. Med.* 362 (2010) 329–344.
- [4] K.P. Kepp, Bioinorganic chemistry of Alzheimer's disease, *Chem. Rev.* 112 (2012) 5193–5239.
- [5] R.A. Marr, D.M. Hafez, Amyloid-beta and Alzheimer's disease: the role of neprilysin-2 in amyloid-beta clearance, *Aging Neurosci.* 6 (2014) 187–93.
- [6] L.M. Ittner, J. Götz, Amyloid- $\beta$  and tau--a toxic pas de deux in Alzheimer's disease, *Nat. Rev. Neurosci.* 12 (2011) 67–72.

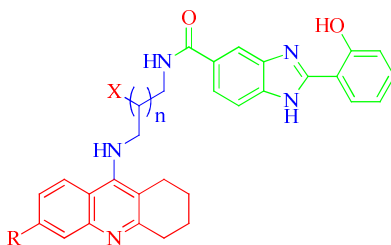
- [7] C.J. Ladner, J.M. Lee, Pharmacological drug treatment of Alzheimer disease: The cholinergic hypothesis revisited, *J. Neuropathol. Exp. Neur.* 57 (1998) 719–731
- [8] V.N. Talesa, Acetylcholinesterase in Alzheimer's disease, *Mech. Ageing Dev.* 122 (2001) 1961–1969
- [9] W.J. Huang, X. Zhang, W.W. Chan, Role of oxidative stress in Alzheimer's disease, *Biomed. Rep.* 4 (2016) 519–522.
- [10] A.I. Bush, R.E. Tanzi, Therapeutics for Alzheimer's disease based on the metal hypothesis, *Neurotherapeutics* 5 (2008) 421–432.
- [11] C. Rodríguez-Rodríguez, M. Telpoukhovskaia, The art of building multifunctional metal-binding agents from basic molecular scaffolds for the potential application in neurodegenerative diseases, *C. Orvig, Coord. Chem. Rev.* 256 (2012) 2308–2332.
- [12] M. A. Santos, K. Chand, S. Chaves, Recent progress in multifunctional metal chelators as potential drugs for Alzheimer's disease, *Coord. Chem. Rev.* 327–328 (2016) 287–303.
- [13] G. Small, R. Bullock, Defining optimal treatment with cholinesterase inhibitors in Alzheimer's disease. *Alzheimer's Dement.* 7 (2011) 177–184.
- [14] J.L. Cummings, T. Morstorf, K. Zhong, Alzheimer's disease drug-development pipeline: few candidates, frequent failures. *Alzheimers Res. Ther.* 6 (2014) 37–43.
- [15] A. Cavalli, M.L. Bolognesi, A. Minarini, M. Rosini, V. Tumiatti, M. Recanatini, C. Melchiorre, Multi-target-directed ligands to combat neurodegenerative diseases, *J. Med. Chem.* 51 (2008) 347–372.
- [16] R. Leon, A.G. Garcia, J. Marco-Contelles, Recent advances in the multitarget-directed ligands approach for the treatment of Alzheimer's disease. *Med. Res. Rev.* 33 (2013) 139–189.

- [17] D. Palanimuthu, R. Poon, S. Sahni, R. Anjum, D. Hibbs, H.-Y. Lin, P.V. Bernhardt, D.S. Kalinowski, D.R. Richardson, A novel class of thiosemicarbazones show multifunctional activity for the treatment of Alzheimer's disease, *Eur. J. Med Chem.* 139 (2017) 612–632.
- [18] M.A. Santos, K. Chand, S. Chaves, Recent progress in repositioning Alzheimer's disease drugs based on a multitarget strategy, *Future Med. Chem.* 8 (2016) 2113–2142.
- [19] M. Decker, *Design of Hybrid Molecules for Drug Development*, Elsevier: USA, 2017.
- [20] M.L. Crismon, Tacrine: first drug approved for Alzheimer's disease, *Ann. Pharmacother.* 28 (1994) 744–751.
- [21] M.G. Savelieff, A.S. DeToma, J.S. Derrick, M.H. Lim, The ongoing search for small molecules to study metal-associated amyloid- $\beta$  species in Alzheimer's disease, *Acc. Chem. Res.* 47 (2014) 2475–2482.
- [22] H. Dvir, I. Silman, M. Harel, T. L. Rosenberry, J. L. Sussman, Acetylcholinesterase: from 3D structure to function, *Chem-Biol. Interact.* 187 (2010) 10–22.
- [23] M.A. Ceshi, J.S. Costa, J.P.B. Lopes, V.S. Câmara, L.F. Campo, A.C.A. Borges, C.A.S. Gonçalves, D.F. Souza, E.L. Konrath, A.L.M. Karl, I.A. Guedes, L.E. Dardenne, *Eur. J. Med. Chem.* 121 (2016) 758–772.
- [24] P. Campos, X. Formosa, C. Galdeano, T. Gomez, D. Muñoz-Torreno, L. Ramirez, E. Viayna, E. Gomez, N. Isamberry, R. Lavilla, A. Badia, M.V. Clos, M. Bartolini, F. Mancini, V. Andrizano, A. Bidon-Chanal, O. Huertas, T. Dafni, F.J. Luque, *Chem.-Biol. Interact.* 187 (2010) 411–515.
- [25] PDB, entry,1ODC. <http://www.rcsb.org/pdb/explore/explore.do?structureId=1ODC>.
- [26] E.H. Rydberg, B. Brumshtein, H.M. Greenblatt, D.M. Wong, D. Shaya, L.D. Williams, P.R. Carlier, Y. Pang, I. Silman, J.L. Sussman, *J. Med. Chem.* 49 (2006) 5491–5500.

- [27] L.J. Sargent, L.J. Small, Attempts to find new antimalarials; studies in the acridine series; dialkylaminoalkylamines derived from 9-chloro-1,2,3,4-tetrahydroacridine, *Org. Chem.* 11 (1946) 359–362.
- [28] M.K. Hu and C.F. Lu, A facile synthesis of bis-tacrine isosteres, *Tetrahedron Lett.* 41 (2000) 1815–1818.
- [29] C. Karthikeyan, V. R. Solomon, H. Lee, P. Trivedi, Synthesis and biological evaluation of 2-(phenyl)-3H-benzo[d]imidazole-5-carboxylic acids and its methyl esters as potent anti-breast cancer agents, *Arabian J. Chem.* 10 (2017) S1788–S1794.
- [30] A. Nunes, S. M. Marques, C. Quintanova, D.F. Silva, S.M. Cardoso, S. Chaves, M.A. Santos, Multifunctional iron-chelators with protective roles against neurodegenerative diseases, *Dalton Trans.* 42 (2013) 6058–6073.
- [31] M. Bartolini, C. Bertucci, M.L. Bolognesi, A. Cavalli, C. Melchiorre, V. Andrisano, Insight into the kinetic of amyloid beta (1-42) peptide self-aggregation: elucidation of inhibitors' mechanism of action, *ChembioChem.* 8 (2007) 2152–161.
- [32] X. Chao, X. He, Y. Yang, X. Zhou, M. Jin, S. Liu, Z. Cheng, P. Liu, Y. Wang, J. Yu, Y. Tan, Y. Huang, J. Qin, S. Rapposelli, Design, synthesis and pharmacological evaluation of novel tacrine–caffeic acid hybrids as multi-targeted compounds against Alzheimer's disease, *Bioorg. Med. Chem. Lett.* 22 (2012) 6498–6502.
- [33] S. Chaves, A. Hiremathad, D. Tomás, R.S. Keri, L. Piemontese, M.A. Santos, unpublished results.
- [34] P. Faller, C. Hureau, Bioinorganic chemistry of copper and zinc ions coordinated to amyloid- $\beta$  peptide, *Dalton Trans.* (2009) 1080–1094.
- [35] A. Conte-Daban, A. Day, P. Faller, C. Hureau, How Zn can impede Cu detoxification by chelating agents in Alzheimer's disease: a proof-of-concept study, *Dalton Trans.* 45 (2016) 15671–15678.

- [36] B. Tepe, D. Daferera, A. Sokmen, M. Sokmen, M. Polissiou, Antimicrobial and antioxidant activities of the essential oil and various extracts of *Salvia tomentosa* Miller (Lamiaceae), *J. Agric. Food. Chem.* 90 (2005) 333–340.
- [37] D.F. Silva, J.E. Selfridge, Lu J, E L, S.M. Cardoso, R.H. Swerdlow. Mitochondrial abnormalities in Alzheimer's disease: possible targets for therapeutic intervention. *Adv Pharmacol.* 64 (2012) 83–126.
- [38] D.F. Silva, J.E. Selfridge, J. Lu, E L, N. Roy, L. Hutfles, J.M. Burns, E.K. Michaelis, S. Yan, S.M. Cardoso, R.H. Swerdlow, Bioenergetic flux, mitochondrial mass and mitochondrial morphology dynamics in AD and MCI cybrid cell lines, *Hum Mol Genet.* 22 (2013) 3931–3946.
- [39] P.H. Reddy, M.F. Beal. Amyloid beta, mitochondrial dysfunction and synaptic damage: implications for cognitive decline in aging and Alzheimer's disease. *Trends in Molecular Medicine*, 14 (2008) 45–53.
- [40] QikProp, version 2.5, Schrödinger, LLC, New York, NY, 2005.
- [41] C.A. Lipinski, F. Lombardo, B.W. Dominy and P.J. Feeney, Experimental and computational approaches to estimate solubility and permeability in drug discovery and development settings, *Adv. Drug Deliv. Rev.* 23 (1997) 3–26.
- [42] Maestro, version 9.3. Schrödinger Inc.: Portland, OR, 2012.
- [43] T. Hassinen, M.J. Peräkylä, New energy terms for reduced protein models implemented in an off-lattice force field, *Comput. Chem.* 22 (2001) 1229–1242.
- [44] M. Clark, R.D. Cramer III, N. Van Opdenbosch, Validation of the general purpose tripos 5.2 force field, *N. J. Comput. Chem.* 10 (2004) 982–1012.
- [45] G. Jones, P. Willett, R.C. Glen, A.R. Leach, R. Taylor, Development and validation of a genetic algorithm for flexible docking, *J. Mol. Biol.* 267 (1997) 727–748.

- [46] C. Quintanova, R.S. Keri, S.M. Marques, M. G-Fernandes, S.M. Cardoso, M.L. Serralheiro, M.A. Santos, Design, synthesis and bioevaluation of tacrine hybrids with cinnamate and cinnamylidene acetate derivatives as potential anti-Alzheimer drugs, *MedChemComm* 6 (2015) 1969–1977.
- [47] J. Sebestík, S.M. Marques, P.L. Falé, M.A. Santos, D.M. Arduíno, S.M. Cardoso, C.R. Oliveira, M.L. Serralheiro, M.A. Santos, Bifunctional phenolic-choline conjugates as anti-oxidants and acetylcholinesterase inhibitors, *J. Enzyme Inhib. Med. Chem.* 26 (2011) 485–497.
- [48] T. Mosmann, Rapid colorimetric assay for cellular growth and survival: application to proliferation and cytotoxicity assays, *J. Immunol. Methods* 65 (1983) 55–63.

**Table 1:** Biological properties of the TAC-BIM hybrids: Anti-oxidant (DPPH), inhibition of AChE and A $\beta_{42}$  aggregation (self- and Cu-induced).

Comp. Code	n	X	R	Antioxid <sup>a</sup> . EC <sub>50</sub> (μM)	AChEInhib <sup>b</sup> IC <sub>50</sub> nM	A $\beta_{42}$ self-aggreg. Inhib <sup>c,d</sup> (%)	A $\beta_{42}$ Cu-ind-aggreg. Inhib <sup>c,d</sup> (%)
11a	0	H	H	-	36.4	40.6	49.4
11b	1	H	H	>1000	30.9	74.6	77.3
11c	2	H	H	-	208.5	57.4	65.5
11d	0	H	Cl	-	6.3	39.4 21.9 <sup>e</sup>	- 20.9 <sup>e</sup>
11e	1	H	Cl	>1000	23.7	50.8	55.8
11f	2	H	Cl	-	142	56.8	-
12a	1	OH	H	564±5	16.8	70.9	59.5
12b	1	OH	Cl	-	18.1	-	-
tacrine	-	-	-	>1000	350 μM	20	--
BIMPhOH				160±3	No Activity	--	--

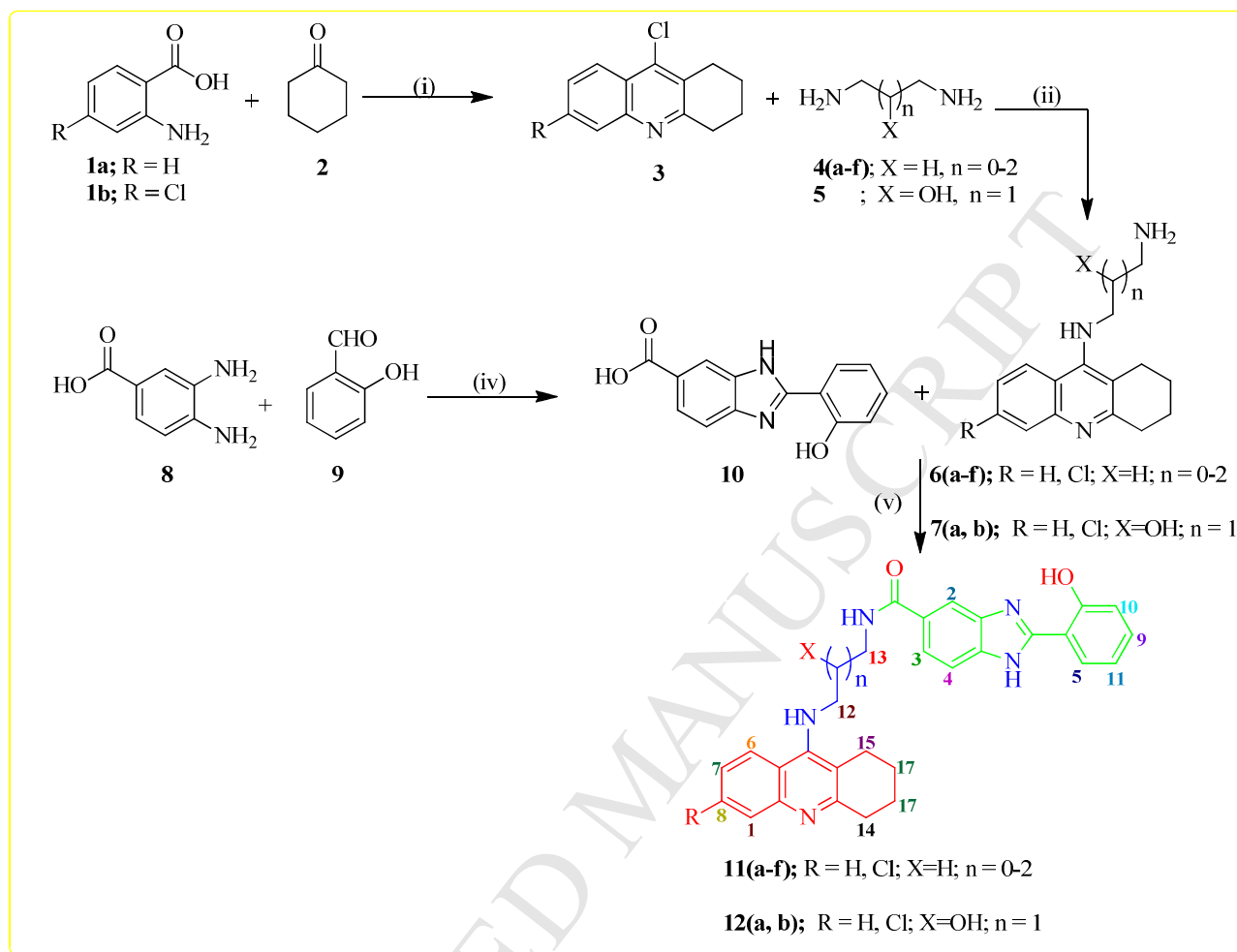
<sup>a</sup>EC<sub>50</sub> values for the DPPH assay, <sup>b</sup>The values are mean of five independent experiments ± SD.

<sup>c</sup>Inhibition of self-mediated A $\beta_{42}$  aggregation (in %) with or without copper (40 μM). The thioflavin-T fluorescence method was used, and the measurements were carried out in the presence of an inhibitor (80 μM). <sup>d</sup>The values are the mean of two independent measurements in duplicate (SEM < 10%). <sup>e</sup> Thioflavin-T fluorescence method in the presence of 40 μM inhibitor.

**Table 2:** Summary of some calculated pharmacokinetic molecular descriptors

<b>code</b>	<b>Molecular Weight</b>	<b>clog <math>P^{a,b}</math></b>	<b>Log <math>BB^{a,c}</math></b>	<b>Caco-2 Permeability (nm/s)<sup>a</sup></b>	<b>Violations of Lipinski rule<sup>a</sup></b>
<b>11a</b>	477.565	4.721	-1.439	400	0
<b>11b</b>	491.591	5.255	-1.507	471	1
<b>11c</b>	505.618	4.826	-1.687	430	2
<b>11d</b>	512.010	5.248	-1.241	457	2
<b>11e</b>	526.036	5.802	-1.320	535	2
<b>11f</b>	540.063	6.078	-1.679	345	2
<b>12a</b>	507.591	4.252	-1.836	268	1
<b>12b</b>	542.036	4.602	-2.030	157	1

<sup>a</sup>Predicted values using program Qikprop v.2.5, <sup>b</sup>Calculated octanol/water partition coefficient, <sup>c</sup>Brain/blood partition coefficient [40].



**Scheme 1:** i)  $\text{POCl}_3$ ,  $180^\circ\text{C}$ , reflux, 4 h; ii) phenol, KI,  $180^\circ\text{C}$ , reflux, 35 min; iii)  $\text{Na}_2\text{S}_2\text{O}_5$ , DMA,  $100^\circ\text{C}$ , reflux 7 h; iv) DCC, NHS, DMF,  $\text{N}_2$  atm., RT, 2 days.

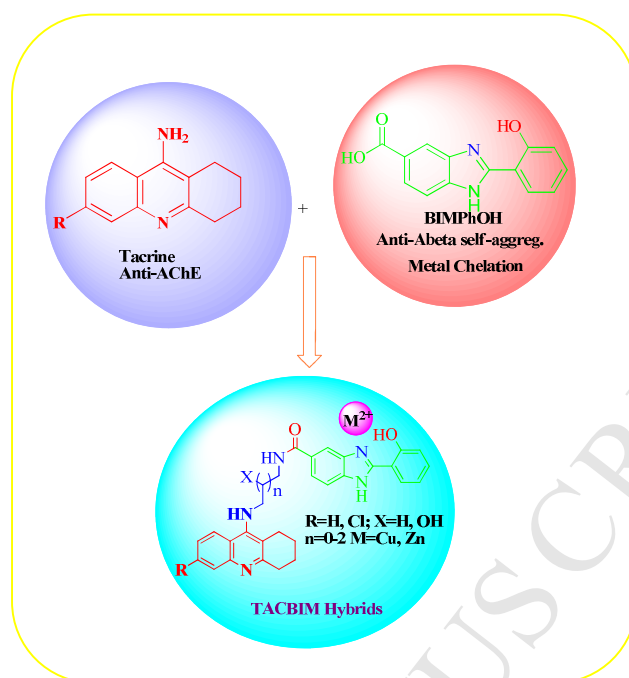


**Fig. 1:** Design of the TAC-BIM hybrids

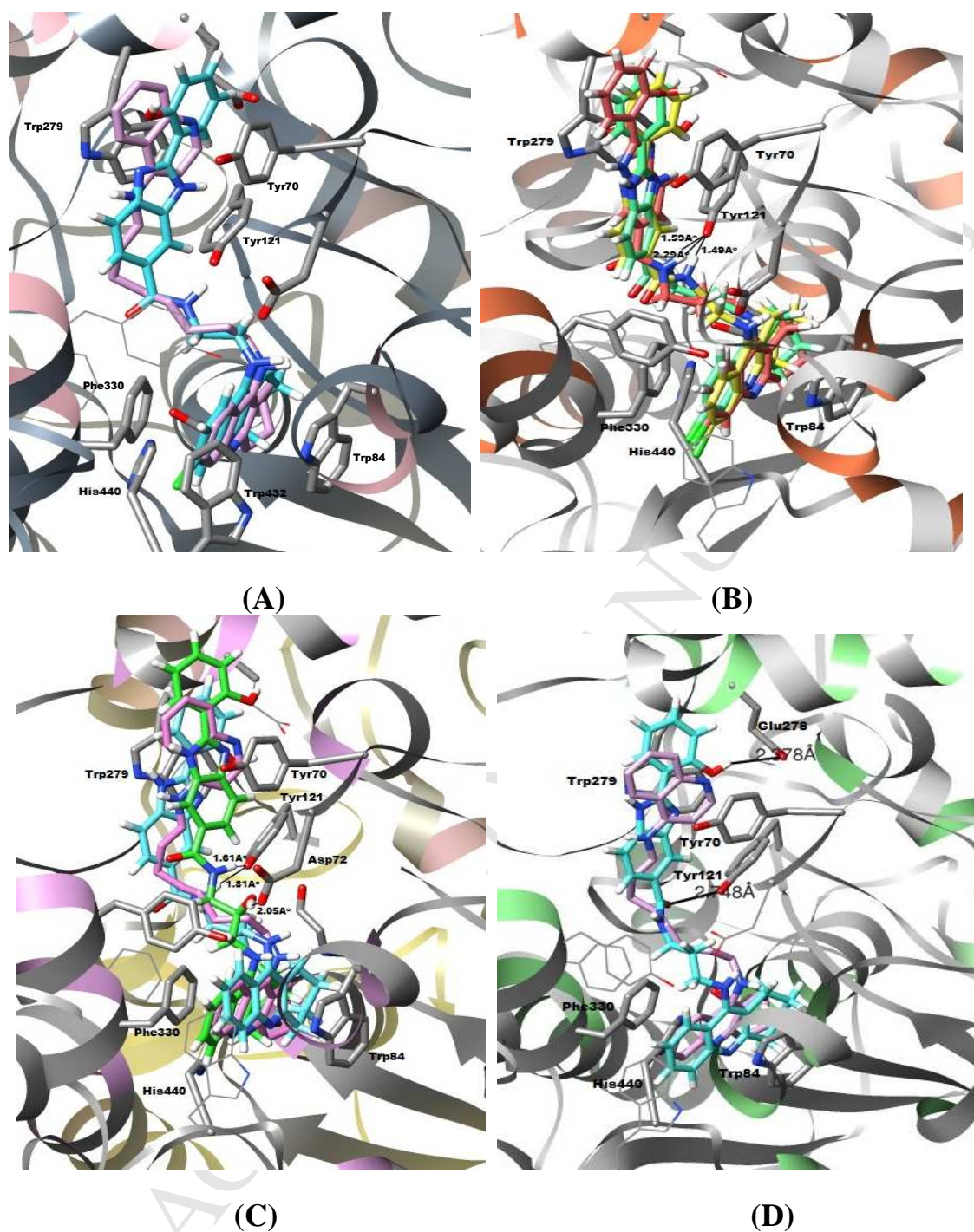


**Figure 2:** Docking results for the TAC-BIM hybrids with *TcAChE*: (A) superimposition of the original ligand (PDB entry 1ODC) (pink) and **11d** (cyan); (B) superimposition of **11d** (yellow) **11e** (light green) and **11f** (red); (C) superimposition of **11b** (cyan) and **12a** (green) with original ligand (pink); (D) superimposition of **11b** (cyan) with original ligand (pink).

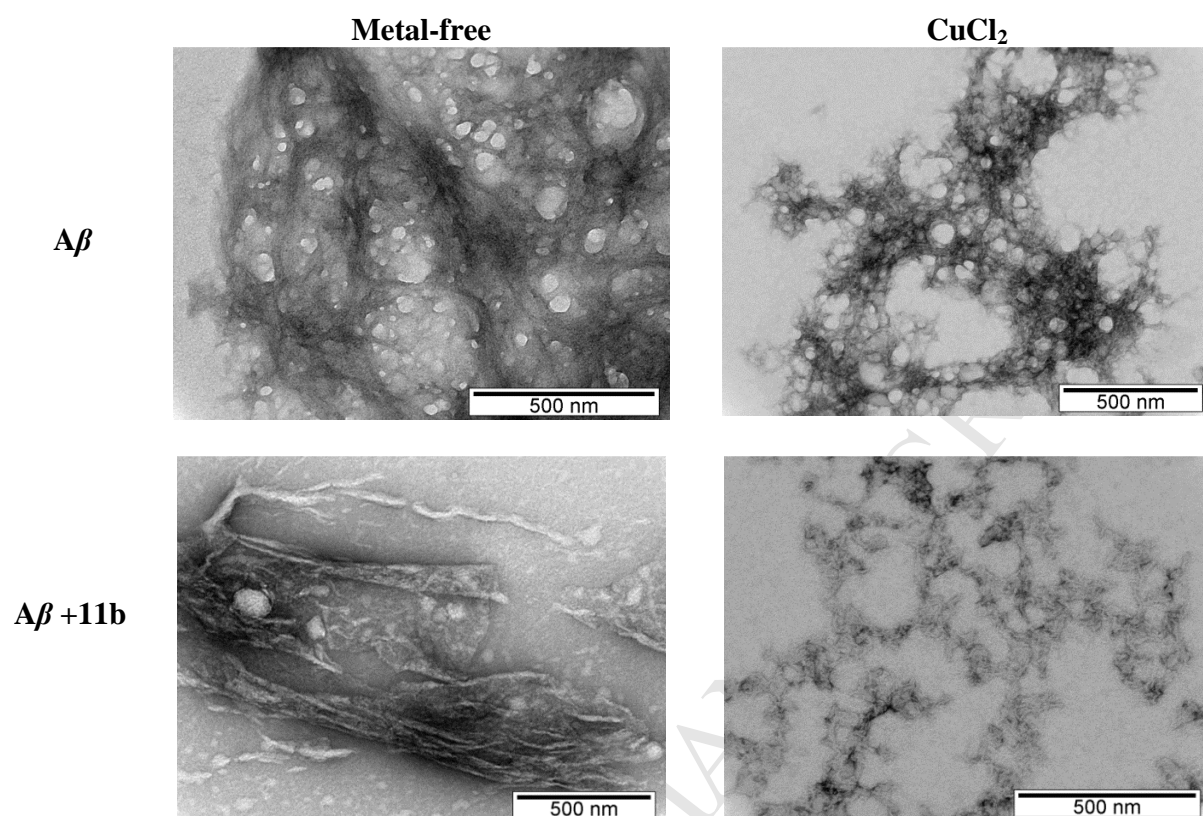


**Fig. 3:** TEM images of  $A\beta$  aggregation inhibition experiments performed with samples incubated (37 °C) for 24 h. Experimental conditions:  $[A\beta_{42}] = [CuCl_2] = 25 \mu M$ ;  $[11b] = 50 \mu M$ ; pH 6.6.

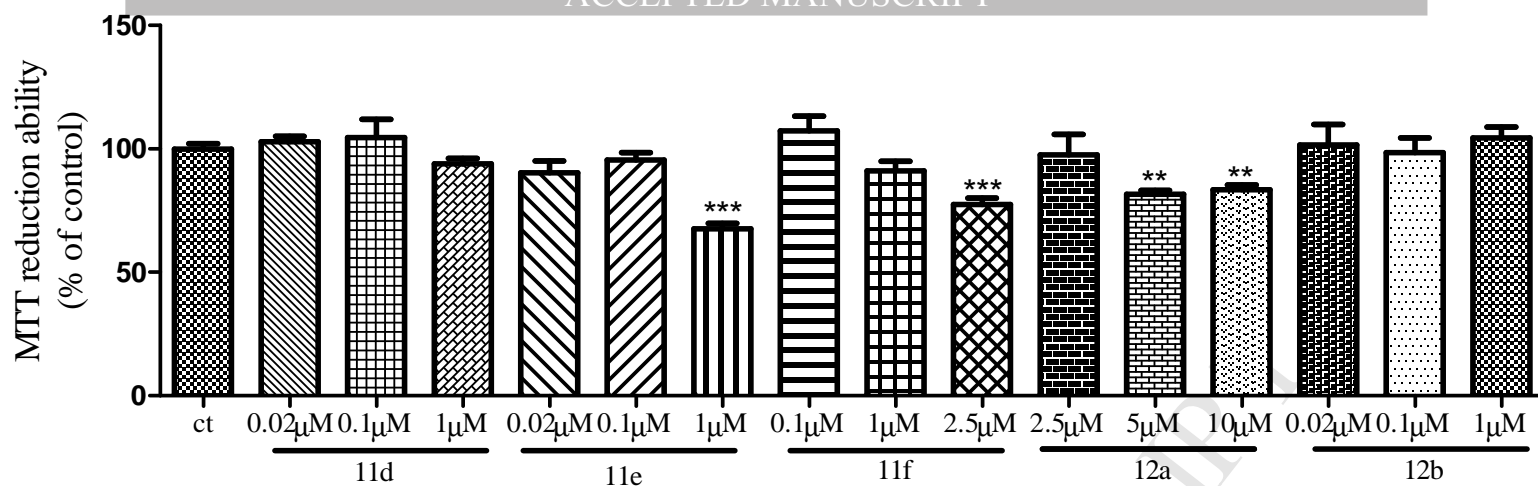


**Fig. 4:** Screening of concentrations of the TAC-BIM hybrid compounds **11d**, **11e**, **11f**, **12a** and **12b** on SH-SY5Y cells. SH-SY5Y cells were treated with the described compounds for 24 h. Evaluation of cell proliferation was determined by using the colorimetric MTT reduction test. Results are expressed as the percentage of SH-SY5Y untreated cells, with the mean  $\pm$  S.E.M. derived from 3 different experiments. \*\* $p < 0.01$  and \*\*\* $p < 0.001$ , significantly different when compared with SH-SY5Y untreated cells.

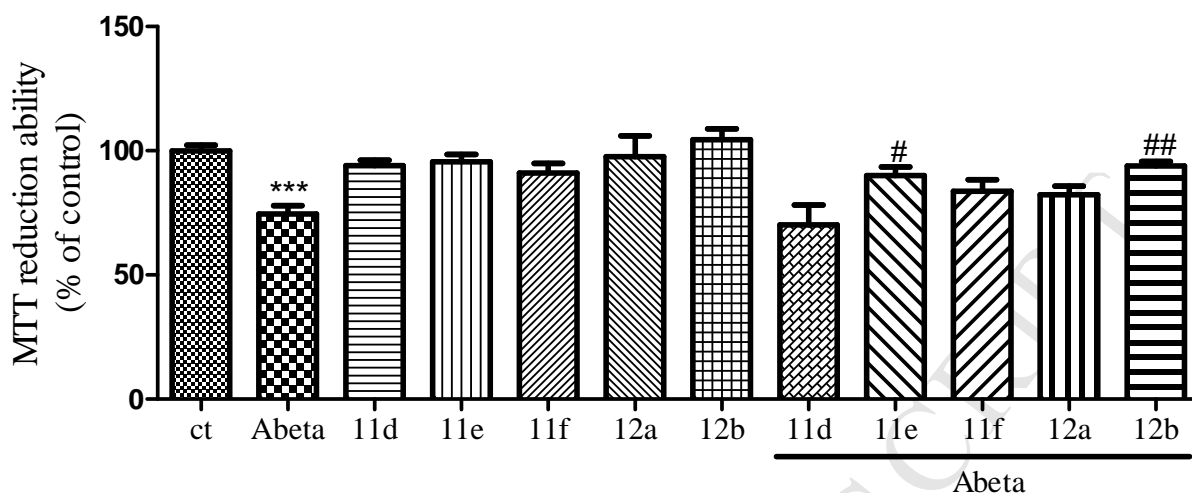


**Fig. 5:** Neuroprotective effect of the TAC-BIM hybrids on  $A\beta_{42}$ -induced toxicity on SH-SY5Y cells. Cells were treated with  $A\beta_{42}$  (Abeta) peptide (1  $\mu$ M), for 24 h after treatment for 1 h in the absence or the presence of the compounds. Evaluation of cell proliferation was performed by using MTT reduction assay. Results are expressed as the percentage of SH-SY5Y untreated cells, with the mean  $\pm$  S.E.M. derived from 3 different experiments. \*\*\* $p < 0.001$ , significantly different when compared with SH-SY5Y untreated cells; # $p < 0.05$  and ## $p < 0.01$ , significantly different when compared with  $A\beta_{42}$  treated SH-SY5Y cells.(concentrations:  $A\beta_{42}$  1  $\mu$ M; **11d**, **11f**, **12b** 1  $\mu$ M; **11e** 0.1  $\mu$ M; **12a** 2.5  $\mu$ M).

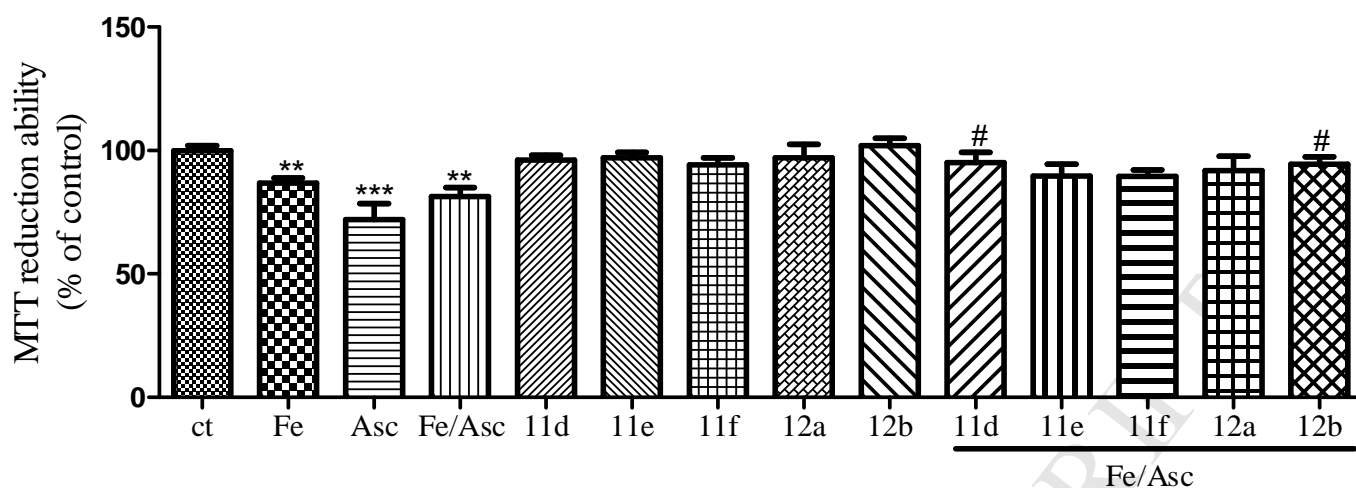


**Fig. 6:** Neuroprotective effect of the TAC-BIM hybrids against Ferrous Sulfate (Fe)/L-Ascorbic Acid (AscH(-)) toxicity on SH-SY5Y cells. Cells were treated with Fe/Asc (500  $\mu$ M/5 mM, respectively) for 24 h, after treatment for 1 h in the absence or the presence of the compounds. Evaluation of cell proliferation was performed by using MTT reduction assay. Results are expressed as the percentage of SH-SY5Y untreated cells, with the mean  $\pm$  S.E.M. derived from 3 different experiments. \*\* $p < 0.01$  and \*\*\* $p < 0.001$ , significantly different when compared with SH-SY5Y untreated cells; # $p < 0.05$ , significantly different when compared with Fe/Asc treated SH-SY5Y cells.

### Highlights

- A novel series of TAC-BIM hybrids as potential anti-AD agents.
- Excellent AChE inhibitors in nanomolar range.
- Good inhibition of self- and Cu-induced A $\beta$  aggregation (up to 75%).
- Radical scavenging and metal chelating capacity.
- Neuroprotection of cell toxicity induced by AD stressors (A $\beta$  and Fe/AsC(-)).